https://doi.org/10.5194/egusphere-2026-3882
Preprint. Discussion started: 27 July 2026

Deciphering the effect of mixing state on ice nucleation using single particle measurements and probabilistic simulations of mixed dust-biological ice nucleating particles

Gavin Cornwell[1], Alla Zelenyuk-Imre[1], Gourihar Kulkarni[1], Nurun Nahar Lata[1], Kaizad Patel[1], Jennifer Yao[1], Zihua Zhu[1], Laura Fierce[1], Payton Beeler[1], Swarup China[1], Isabelle Steinke[1,2], and Susannah Burrows[1]

[1]Pacific Northwest National Laboratory, Richland, WA 99354.
[2]Delft University of Technology, Delft, The Netherlands.

Correspondence: Gavin Cornwell (gavin.cornwell@pnnl.gov)

Abstract. Ice-nucleating particles (INPs) in soils are complex mixtures of mineral dust and biological material, yet the influence of particle mixing state on ice nucleation activity remains poorly constrained. Here, we generated synthetic soils using montmorillonite and Snomax to evaluate the suitability of current analytical methods for characterizing and predicting the ice nucleation activity of complex particle mixtures. Particle composition was characterized using single particle mass spectrometry (SPMS) and computer controlled scanning electron microscopy with electron dispersive x-ray (CCSEM/EDX), as well as Time-of-Flight Secondary Ion Mass Spectrometry (ToF-SIMS) for surface chemical analysis. Ice nucleation experiments were conducted using a Continuous Flow Diffusion Chamber (CFDC). CCSEM/EDX classified particles predominantly as externally mixed while SPMS demonstrated greater sensitivity to Snomax and identified more internally-mixed particles. Residual particles from both techniques showed enhanced biological markers compared to the bulk population. Frozen fractions did not scale with mass mixing ratios, and simulations indicated that mixing state had minimal effect on ice nucleation activity when total Snomax mass was conserved. We also found some limited evidence that incorporating particle mixing state from measurements improves simulated frozen fractions. These results demonstrate that accurate prediction of INP activity in dust-biological mixtures requires constraints on the abundance and particle-level distribution of active biological material, rather than bulk or population-average compositional descriptions alone.

1 Introduction

Ice nucleating particles (INPs) affect cloud radiative properties and precipitation through their ability to initiate primary ice formation. Primary ice formation is a critical step required for many important cloud microphysical processes, such as secondary ice production (SIP) processes (e.g., Hallett-Mossop rime splintering), whose combined effects ultimately govern mixed-phase cloud properties USDOE Office of Science (SC), Biological and Environmental Research (BER) et al. (2026). The ice nucleation (IN) activity of aerosol varies dramatically between different particle types (Kanji et al., 2017), so accurately predicting INP concentrations requires that even low-concentration particle types be represented, provided they possess a sufficiently

https://doi.org/10.5194/egusphere-2026-3882
Preprint. Discussion started: 27 July 2026

high ice nucleation activity (e.g. Cornwell et al., 2023). Thus, model prediction of INP concentrations and variability requires aerosol-aware schemes that are able to account for this inherent variance in IN activity.

As outlined by Burrows et al. (2022), using aerosol-aware INP parameterizations in cloud microphysics schemes requires complex treatment of modeled aerosol because of the diversity of particle properties that affects IN-activity. Many models now employ simplified representations of aerosol composition, though our ability to model aerosol composition is still unable to represent IN-relevant information such as morphology and/or mixing state. The mixing state is the distribution of species across the particles in the population (Riemer et al., 2019). A population is a fully internal mixture if all particles in the population contain the same species in the same mass fractions, while a population is an external mixture if every particle contains just one species. For the rest of this manuscript, when we refer to a population as being internally or externally mixed, we assume that these systems are fully internally or externally mixed, unless noted otherwise. We do not have a full understanding of how the mixing state in complex particle systems affects ice nucleation activity. For instance, laboratory studies have shown that organic-rich dusts are more active INPs compared to mineral dusts, and that greater IN activity can be correlated with the organic content across bulk soil samples (Conen et al., 2011). Other studies have shown a link between atmospheric aging and IN-activity, though the magnitude and direction of the effect varies by particle type and aging process (e.g. Kulkarni et al., 2014, 2015; Augustin-Bauditz et al., 2014; Gute et al., 2020; Jahl et al., 2021). We note that these studies do not necessarily distinguish between internal mixing state and the effects of chemical changes induced by the aging process. This raises the question: *do we have the measurement capabilities and conceptual framework required to predict the ice nucleation activity of mixed particles given a sufficiently complete description of the population level properties?*

There are few laboratory studies that have attempted to predict total ice nucleation activity for complex mixtures of particles. Beydoun et al. (2017) used mixtures of Snomax and illite in droplet freezing assays to study how particle mixing state affects the ice nucleation activity of organic-rich soils. They used mass mixing ratios as an approximation of the mixing state, and found that a multi-component ice nucleation scheme fit their experimental results well, though we note that droplet freezing assays may not be as well suited for measuring internally mixed particles. Augustin-Bauditz et al. (2016) measured the ice nucleation activity of particles aerosolized from an aqueous mixture of illite and birch pollen washing water (a known source of biological ice macromolecules) using a laminar diffusion tube cloud chamber. They characterized the mixing state of particles using single particle and growth factor measurements, which they used as input for a multi-component ice nucleation model that was able to accurately describe the freezing activity of their mixed particles. However, they were unable to detect biological components in their single particle measurements, significantly limiting the applicability of their approach to ambient measurements. Finally, neither study measured the composition of the ice nucleating particles to verify closure between particle composition and IN activity. We posit that verifying the composition of INPs, and not just the frozen fraction of freezing assays, is a critical step which is often neglected.

To meet this need, we generated synthetic soils using montmorillonite and Snomax for use in ice nucleation experiments. Model systems of mixed dust and biological particles have clear advantages for studying mixing state effects on ice nucleation. First, they have very different ice nucleation behaviors, and they are relatively straightforward to distinguish in ice nucleation experiments. Second, dust is a common ice nucleator in the atmosphere, and Snomax is frequently used as a proxy for ice nu-

https://doi.org/10.5194/egusphere-2026-3882
Preprint. Discussion started: 27 July 2026

cleating proteins, and thus we think that these measurements have some real-world applicability. We measured the composition of synthetic soils, along with the INP composition, using single particle techniques. We used single particle mass spectrometry (SPMS) and computer-controlled scanning electron microscopy with energy dispersive spectroscopy (CCSEM/EDX) because these are the two commonly used methods for identifying unknown particle populations in ambient measurements. Surface chemistry was also measured using time-of-flight secondary ion mass spectrometry (ToF-SIMS). We also measured the ice nucleation activity using a continuous flow diffusion chamber (CFDC). Finally, we used a probabilistic approach to simulate the freezing of these synthetic soils in the CFDC, and discuss the implications for future research needs.

2 Materials and Methods

2.1 Artificial soil formulation

We generated synthetic soils designed to mimic organic-rich agricultural soils, which have been identified in previous studies as efficient INPs (Tobo et al., 2014; Hill et al., 2016). We produced a two-component system in which montmorillonite and Snomax were used to simulate the dust and organic components respectively. Montmorillonite is a clay mineral widely used in ice nucleation studies (e.g., Conen et al., 2011), and has a high cation exchange capacity that enables metabolites to strongly adsorb to surfaces (Zhu et al., 2019). Snomax (Snomax International) is a commercially available, very efficient ice nucleator derived from cultures of *Pseudomona Syringae*, and is widely used in ice nucleation studies as a proxy for bioparticles with ice nucleation activity at warm temperatures (Wex et al., 2015). The warm temperature IN-activity of Snomax has been tied to three different protein complexes, which are believed to be aggregates of ice nucleating protein momomers of various size, and are active at temperatures warmer than -15 °C.

To prepare the synthetic soils, we took 50 g Snomax and ground it using a mortar and pestle. We weighed out an appropriate amount of Snomax for each sample and dissolved it in 100 mL of water. Then we weighed 100 g montmorillonite (montmorillonite K10) into Nalgene bottles and added the Snomax solution to the bottle. Samples were placed on a horizontal shaker, set at 200 rpm, for 24 hours to facilitate the adsorption of Snomax particles onto montmorillonite. After shaking, we transferred the mixtures to 500 mL glass beakers and let them air dry in a fume hood for one week. We transferred the air-dried material to 50 mL centrifuge tubes, filling each tube approximately 1/3 full. Note that this necessitated multiple tubes per sample. Centrifuge tubes were freeze-dried overnight, combined into a single sample, and finally ground using a mortar and pestle. Pure montmorillonite and Snomax samples were processed similarly to control for potential confounding effects on particle composition and/or ice nucleation activity.

2.2 Experimental setup

Figure 1 shows the experimental setup for these experiments. Montmorillonite and mixed montmorillonite-Snomax particles were dry-generated using a dry powder generator (SAG 410/U, from TOPAS GmbH), and aerosolized into a 5 L stainless steel chamber. Snomax particles were dry suspended in a 100 L teflon filled with filtered air. We did not use the Teflon bag for dust

https://doi.org/10.5194/egusphere-2026-3882
Preprint. Discussion started: 27 July 2026

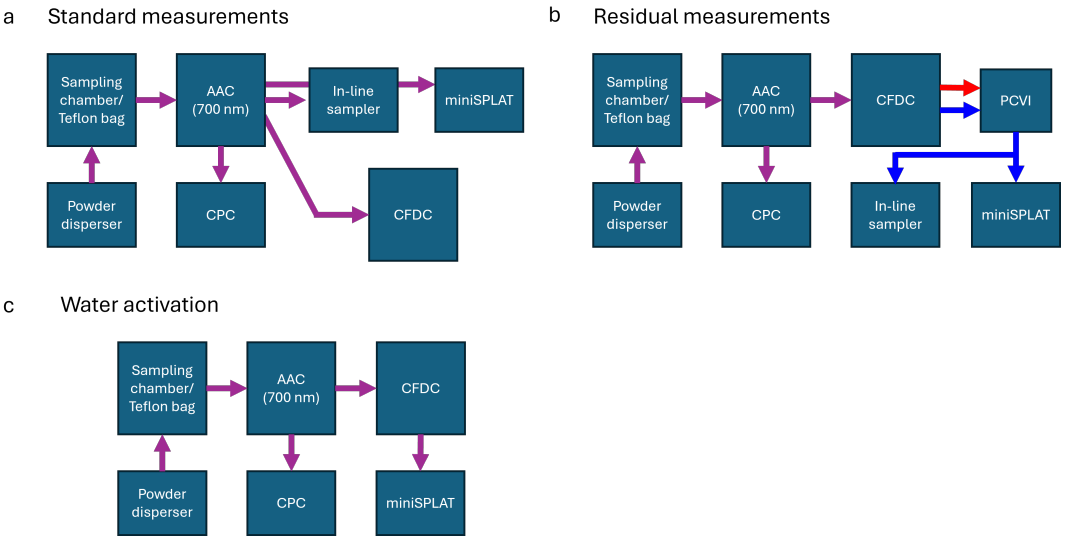

Figure 1. Experimental setup for the characterization of the synthetic soils for the three different operation modes (a) standard measurements, (b), residual measurements, and (c), water activation. Purple lines indicate sampling lines that contain both INPs and non-INPs, while blue and red lines indicate sampling lines that contain only INPs and un-activated particles, respectively.

and synthetic soil particles because of rapid wall losses, thus explaining the different aerosolization methods. Due to the large amounts of particles generated by the dry powder generator and the small volume of the steel chamber, it was necessary to periodically pulse dust into the chamber rather than run it continuously. In contrast, the Snomax particles could be sampled continuously. Particles were sampled from either the stainless steel chamber or the teflon bag, and size-selected at 700 nm using the aerodynamic aerosol classifier (AAC; Cambustion Ltd), using a sheath flow of 5.5 LPM, a sample flow of 1.0 LPM, and a resolution of 10. Using an AAC to size select particles, as opposed to a differential mobility analyzer, offers a few distinct advantages. First, it is easier to sample larger particles, which are generally expected to be more efficient INPs due to their greater surface area. Second, there are no multiply charged particles, which can skew frozen fraction measurements because they are larger than singly charged particles. Finally, classifying via aerodynamic diameter facilitates the calculation of particle effective density (ρ_{eff}), a key parameter in our simulations.

We employed three distinct measurement modes to characterize samples: (1) standard measurements, (2) residual measurements, and (3) water activation. We used the standard measurements (hereafter "standards") to determine the single particle composition and ice nucleation (IN) activity of size-selected particles from each sample. These measurements were collected using the miniSPLAT, CFDC, and an in-line aerosol sampler that uses copper lacey grids. Offline samples were analyzed after the experiments using electron microscopy (see Section 2.3.1). The residual mode measurements were used to determine the INP composition for each sample. In this mode, particles that induced nucleation of ice and became large ice crystals in the CFDC were separated from interstitial particles using a pumped counterflow virtual impactor (PCVI; Boulter et al., 2006; Kulkarni et al., 2011). Residuals were measured by the single particle mass spectrometer (miniSPLAT) and collected on copper

https://doi.org/10.5194/egusphere-2026-3882
Preprint. Discussion started: 27 July 2026

lacey grids using the in-line aerosol sampler. Finally, water activation experiments were performed to probe the effects that droplet activation and sample preparations had on particle size, shape, and composition. In these experiments, the temperature of evaporation section of the CFDC was fixed (~-10 °C) to ensure supercooled droplets formed within the nucleation section of the chamber do not freeze. These supercooled droplets that exited the CFDC were dried and droplet residuals were analyzed using miniSPLAT (Fig. 1c). The purpose of these experiments was to disentangle what role droplet formation/evaporation had on the residual particle size, shape, and composition.

2.3 Particle composition

We provide particle composition information using three measurement techniques: (1) electron microscopy, (2) single particle mass spectrometry, and (3) time-of-flight secondary ion mass spectrometry (ToF-SIMS).

2.3.1 CCSEM/EDX

Size-resolved chemical composition of particles were characterized using CCSEM/EDX (Quanta 3D, Thermo Fisher) at the Environmental Molecular Sciences Laboratory (EMSL) (Laskin et al., 2006). The CCSEM was equipped with an FEI Quanta digital field emission gun operated at 20 KV and 480pA. CCSEM/EDX analysis reports particle size as the projected area equivalent diameter (AED), with corresponding EDX spectra for each particle (Lata et al., 2021; Cheng et al., 2022; Laskin, 2011). The relative atomic fractions of 15 elements (C, N, O, Na, Mg, Al, Si, P, S, Cl, K, Ca, Mn, Fe, and Zn) were calculated using EDX spectra and particles were classified into five different types the classification scheme described in Table 1 and statistics for the particles classified by the CCSEM/EDX are shown in Table 2.

Class	Criteria
Biological	[P] $\geq$ 0.5% and [MD] < 4%,
Dust and biological	[P] $\geq$ 0.1% and [MD] $\geq$ 4%,
Processed biological	[P] < 0.5% and [CNO] $\geq$ 96% and [MD] < 4%,
Processed dust and biological	[P] < 0.5% and [CNO] $\geq$ 96% and [MD] $\geq$ 1%,
Dust	[P] < 0.5% and [CNO] < 96%,

Table 1. Particle classification criteria for particles measured by CCSEM/EDX. Here, [MD] = Mineral Dust = sum [Ca, Al, Si, Fe].

2.3.2 miniSPLAT

Principle of operation

Size-resolved composition of individual particles was measured by the miniSPLAT. In brief, particles are introduced to an aerodynamic lens, which collimates the particle beam to optimize transmission through the rest of the instrument. The pressure in the aerodynamic lens is partially governed by a critical orifice (CO). The miniSPLAT is typically operated using a 100 µm CO to optimize the particle transmission efficiency between 100 and 600 nm (Zelenyuk et al., 2009). In this study, we

https://doi.org/10.5194/egusphere-2026-3882
Preprint. Discussion started: 27 July 2026

Sample	Biological	Dust and biological	Processed biological	Dust and processed biological	Dust	Total
Snomax bulk	494 (0.707)	0	205 (0.293)	0	0	699
10:1 SS bulk	29 (0.093)	8 (0.026)	21 (0.068)	0	253 (0.814)	311
100:1 SS bulk	4 (0.001)	18 (0.006)	132 (0.044)	4 (0.001)	2810 (0.947)	2968
1000:1 SS bulk	0	10 (0.009)	21 (0.019)	1 (0.001)	1081 (0.971)	1113
100,000:1 SS bulk	5 (0.003)	4 (0.003)	13 (0.009)	5 (0.003)	1469 (0.982)	1496
Dust bulk	0	1 (0.001)	0	0	969 (0.999)	970
Snomax residual (-34 °C)	316 (0.938)	0	21 (0.062)	0	0	337
10:1 SS residual (-34 °C)	n/a	n/a	n/a	n/a	n/a	n/a
100:1 SS residual (-34 °C)	0	253 (0.751)	16 (0.047)	1 (0.003)	100 (0.297)	370
1000:1 SS residual (-34 °C)	1 (0.001)	994 (0.708)	4 (0.003)	3 (0.002)	402 (0.286)	1404
100,000:1 SS residual (-34 °C)	0	40 (0.69)	3 (0.052)	0	15 (0.259)	58
Dust residual (-34 °C)	n/a	n/a	n/a	n/a	n/a	n/a
Snomax residual (-20 °C)	n/a	n/a	n/a	n/a	n/a	n/a
10:1 SS residual (-20 °C)	0	16(0.552)	2 (0.069)	3 (0.103)	8 (0.276)	29
100:1 SS residual (-20 °C)	n/a	n/a	n/a	n/a	n/a	n/a
1000:1 SS residual (-20 °C)	4 (0.053)	61 (0.803)	0	1 (0.013)	10 (0.132)	76
100,000:1 SS residual (-20 °C)	n/a	n/a	n/a	n/a	n/a	n/a
Dust residual (-20 °C)	n/a	n/a	n/a	n/a	n/a	n/a

Table 2. Particle class statistics for lab samples measured by CCSEM/EDX. Both the total number and (fraction) are provided.

followed the work of Cornwell et al. (2024) and we used a 200 µm CO to increase the transmission efficiency for particles with a diameter > 600 nm. The particle beam passes through two optical detection stages set at a fixed distance. The time difference between light scattering events at the two detectors is used to determine the velocity of the particles, which is converted to vacuum aerodynamic diameter (D_{va}) through external calibration using polystyrene latex spheres. The particle velocity is also used to trigger an excimer laser (193 nm; 1.0-1.2 mJ pulse^{-1}) to desorb and ionize the particle. Ions are introduced to a dual-polarity Z-configuration reflectron time-of-flight mass spectrometer. Raw time-of-flight spectra collected by the miniSPLAT were reduced into single m/z spectra and processed spectra were imported into the Matlab software package FATES (Sultana et al., 2017).

Particle classification schemes.

In contrast to SPMS field studies (e.g. Martin et al. (2017); Gunsch et al. (2017), we do not use unsupervised methods to classify our particles. Rather, given the methods used in creating our particle populations, we assumed that particles could be classified into dust, Snomax, or mixed. We determined that using the summed peak areas for $84^{+}, 86^{+}$ was a good indicator for Snomax because it was present in nearly all Snomax particles and much less so in dust (see Section 3.1 for more details). These peaks have been previously attributed to leucine, an amino acid, and are thus likely a marker for proteins in these

https://doi.org/10.5194/egusphere-2026-3882
Preprint. Discussion started: 27 July 2026

measurements (Cornwell et al., 2022). We also determined that $98^+/100^+$ was a good representative peak for dust, but this peak disappears upon wetting in the CFDC and is therefore not suitable for classifying particles across all experiments. Particles with $log_{10}(84^+,86^+)$ greater than the 0.0891 and were classified as Snomax, while particles with $log_{10}(84^+,86^+)$ less than 0.0272 were classified as dust. Particles with a $log_{10}(84+,86^+)$ between 0.0891 and 0.0272 were classified as mixed. These thresholds were determined from the pure dust and Snomax spectral data for these peaks (Fig. 4).

Sample	Dust	Internally-mixed	Snomax	Total	ρ_{eff}
Snomax bulk	1 (0.001)	0 (0.000)	1549 (0.999)	1550	0.612 ± 0.157
10:1 SS bulk	15 (0.042)	43 (0.121)	296 (0.836)	354	0.582 ± 0.173
100:1 SS bulk	52 (0.161)	118 (0.366)	152 (0.472)	322	0.562 ± 0.718
1000:1 SS bulk	39 (0.476)	30 (0.366)	13 (0.159)	82	0.448 ± 0.168
100,000:1 SS bulk	321 (0.961)	11 (0.033)	2 (0.006)	334	0.501 ± 0.180
Dust bulk	306 (1.000)	0 (0.000)	0 (0.000)	306	0.474 ± 0.192
Snomax residual (-34 °C)	0 (0.000)	0 (0.000)	1124 (1.000)	1124	1.008 ± 0.237
10:1 SS residual (-34 °C)	12 (0.059)	1 (0.005)	190 (0.936)	203	0.716 ± 0.451
100:1 SS residual (-34 °C)	43 (0.141)	93 (0.305)	169 (0.554)	305	0.631 ± 0.196
1000:1 SS residual (-34 °C)	110 (0.547)	66 (0.328)	25 (0.124)	201	0.604 ± 0.184
100,000:1 SS residual (-34 °C)	87 (0.956)	4 (0.044)	0 (0.000)	91	0.656 ± 0.207
Dust residual (-34 °C)	58 (0.935)	2 (0.032)	2 (0.032)	62	0.612 ± 0.168
Snomax residual (-20 °C)	1 (0.001)	0 (0.000)	1120 (0.999)	1121	1.079 ± 0.218
10:1 SS residual (-20 °C)	0 (0.000)	0 (0.000)	94 (1.000)	94	0.612 ± 0.154
100:1 SS residual (-20 °C)	39 (0.154)	5 (0.020)	209 (0.826)	253	0.657 ± 0.493
1000:1 SS residual (-20 °C)	19 (0.452)	3 (0.071)	20 (0.476)	42	0.592 ± 0.264
100,000:1 SS residual (-20 °C)	3 (0.750)	1 (0.250)	0 (0.000)	4	0.380 ± 0.149
Dust residual (-20 °C)	2 (1.000)	0 (0.000)	0 (0.000)	2	1.798 ± 1.781

Table 3. Particle statistics for lab samples measured by the miniSPLAT. First three columns show the number (fraction) of particles classified as dust, internally-mixed, or snomax. ρ_{eff} refers to effective density, and is given as the mean ± standard deviation.

2.3.3 ToF-SIMS

We performed ToF-SIMS measurements of the synthetic soils using a TOF. SIMS 5 instrument (IONTOF GmbH, Münster, Germany). Sample preparation details and instrument parameters have been described previously (Huang et al., 2021). In brief, a 25 keV pulsed bismuth (Bi_3^+) primary ion beam, focused to ~ 5 μm in diameter, was rastered over a 500 × 500 μm^2 area on sample that was collected on indium foil. The instrument was operated in high mass resolution mode, with a raster resolution of 128 × 128 pixels. Both positive and negative ion spectra were acquired from each region of interest (ROI), with 5–6 ROIs analyzed per sample. Data reconstruction was performed using SurfaceLab 6 software (version 6.3, IONTOF GmbH). The mass resolution ranged from 3000 to 5000. Mass calibration was performed using the following peaks $^{15}CH_3^+$, $^{55}C_4H_7^+$, and

https://doi.org/10.5194/egusphere-2026-3882
Preprint. Discussion started: 27 July 2026

$^{69}C_4H_7N^+$ for positive spectra, and $^{13}CH^-$, $^{25}C_2H^-$, and $^{97}SO_4H^-$ for negative spectra. Following Zhou et al. (2024), we applied Principal Component Analysis (PCA) to all mass spectra collected from all samples.

2.4 Ice nucleation activity

We used the Pacific Northwest National Laboratory's continuous flow diffusion chamber (PNNL-CFDC; Kulkarni et al., 2020) to both quantify sample ice nucleation activities, as well as to activate aerosol into ice crystals for residual measurements. This ice chamber has been described before, so here we provide only a short overview of its design and operation. Particles are introduced to the instrument through an inlet wherein they are dried using silica diffusion driers before entering the main chamber. The main chamber has a parallel plate geometry; both plates coated with a thin layer of ice and split into two thermally distinct sections. The first section of the chamber is held at sufficiently high supersaturations such that all aerosol particles activate into droplets. The second section is held at cold temperatures with no temperature gradient such that two things occur: (1) droplets containing INPs can freeze into ice crystals and (2) the ice saturated conditions causes unfrozen droplets to completely evaporate. This unique principle of operation unambiguously distinguishes between ice crystals and interstitial particles.

The PNNL-CFDC was configured in two different modes. The first configuration ("residual-mode") was used to nucleate aerosol into droplets/ice crystals so that they could be isolated for measurement. In this configuration, the exhaust of the CFDC was routed to a pumped counterflow virtual impactor (PCVI; Brechtel Manufacturing Inc.), which uses a counterflow to separate particles on the basis of their inertia. Practically, this facilitates the isolation of activated droplets/ice crystals because these are substantially larger than un-activated particles. The second configuration ("fraction-mode") was used to quantify the frozen fraction for ice nucleation experiments. During this configuration, the CFDC was equipped with an optical particle counter (OPC) instead of the PCVI. Both un-activated particles and ice crystals are sized by the OPC and particles larger than 3 µm are determined to be ice crystals. To quantify the ice nucleation activity of each sample, we calculate the frozen fraction (f) as

$$f = \frac{N_{\mathrm{INP}}}{N_{\mathrm{CPC}}} \tag{1}$$

where N_{INP} is the number of particles detected by the OPC that are larger than 3 µm, and N_{CPC} is the total number of particles detected by the condensation particle counter (TSI Inc., TSI 3775; CPC). The CPC was used upstream and downstream of the CFDC to understand particle losses, and this loss factor was used to correct f.

2.5 Simulations of INP measurements

We follow the methodology of Alpert and Knopf (2016) to probabilistically simulate isothermal ice nucleation experiments in order to understand how mixing state affects ice nucleation activity. This approach allows us to account for the effects of variable size, surface area, or composition-related ice nucleation efficiency within a single droplet (e.g. Knopf et al., 2020). We describe this approach in brief below, please see Alpert and Knopf (2016) for more details.

https://doi.org/10.5194/egusphere-2026-3882
Preprint. Discussion started: 27 July 2026

We simulate the isothermal freezing of an ensemble of droplets within the PNNL-CFDC. Each droplet is assumed to have one and only one particle inside. The probability of droplet j from the ensemble freezing, $P_{j,\text{frz}}$, can be given by the following

$$P_{j,\text{frz}} = 1 - e^{-J_{\text{het}} A_j \Delta t} \tag{2}$$

where J_{het} is the heterogeneous freezing coefficient, A_j is the total surface area for particle j, and Δt is the time frame over which freezing is evaluated. J_{het} is a time and surface area dependent measure of the particle ice nucleation activity, and is a function of the measurement temperature and the particle composition. The determination of J_{het} for dust and Snomax is described in Appendix C. A_j is randomly selected from a distribution of aerodynamic diameters, which was simulated by assuming a log-normal distribution, a mean aerodynamic diameter selected by the AAC (700 nm), and a geometric standard deviation of 1.2. Using these parameters, we were able to generate a distribution that matched well with measurements collected by an Aerodynamic Particle Sizer (APS, Tsi Inc.; see Figure B1). We then converted the aerodynamic diameter to physical diameter using ρ_{eff} for each bulk synthetic soil (Table 3). Finally, we used a δt of 0.1 seconds and a total residence time in the instrument of 5 s (Kulkarni et al., 2011).

Each experiment consisted of 10,000 particle members, and was repeated 10 times. The temperature for each experiment was determined to be fixed, and separate experiments used to determine frozen fractions from 239 to 255 K, in one degree increments.

3 Results and discussion

3.1 single particle composition

We measured the composition of size-selected synthetic soil particles using two single particle techniques. single particle techniques are particularly advantageous for studying INP composition because they are able to discern the mixing state of individual particles and facilitate the separation of residuals from interstitial particles. We classified particles measured by CCSEM/EDX into five categories based upon their elemental composition, which we further narrow into three categories: (1) Bio, (2) Bio + Dust, and (3) Dust. Unsurprisingly, the pure samples (i.e. Snomax and dust) are comprised of either Bio or Dust, and not internal mixtures (Fig. 2a). We had expected that, due to the fact that the synthetic soils were created in solution, all of the particles would be internally mixed, with most particles containing a mixture of Bio and Dust. However, the synthetic soils, as classified by CCSEM/EDX, were primarily externally mixed, with most particles containing a single component rather than a mixture of Dust + Bio. For example, the 10:1 synthetic soil was only 2.6% Bio + Dust (internally mixed), and 81.4% Dust and 16.1% Bio (both externally mixed). These results from CCSEM/EDX suggest that our experimental methodology for generating synthetic soils yielded particle populations that were primarily externally-mixed.

In addition to standard measurements of synthetic soils, we also used a PCVI to select ice crystal residuals from the exhaust of the PNNL-CFDC and measured the physicochemical properties of these particles using CCSEM/EDX and miniSPLAT. Unfortunately, we were unable to get sufficient sample to characterize the INP composition for some of the CCSEM/EDX samples due to particle losses during the transmission of particles through the PCVI, and thus our analysis here is incomplete.

https://doi.org/10.5194/egusphere-2026-3882
Preprint. Discussion started: 27 July 2026

Overall, residual particles measured by CCSEM/EDX had more biological material on them compared to the standard particles (Table D1), and which is also reflected by the increase in particles classified as 'Bio' or 'Bio + dust', which is more pronounced at higher temperatures (Fig. 2).

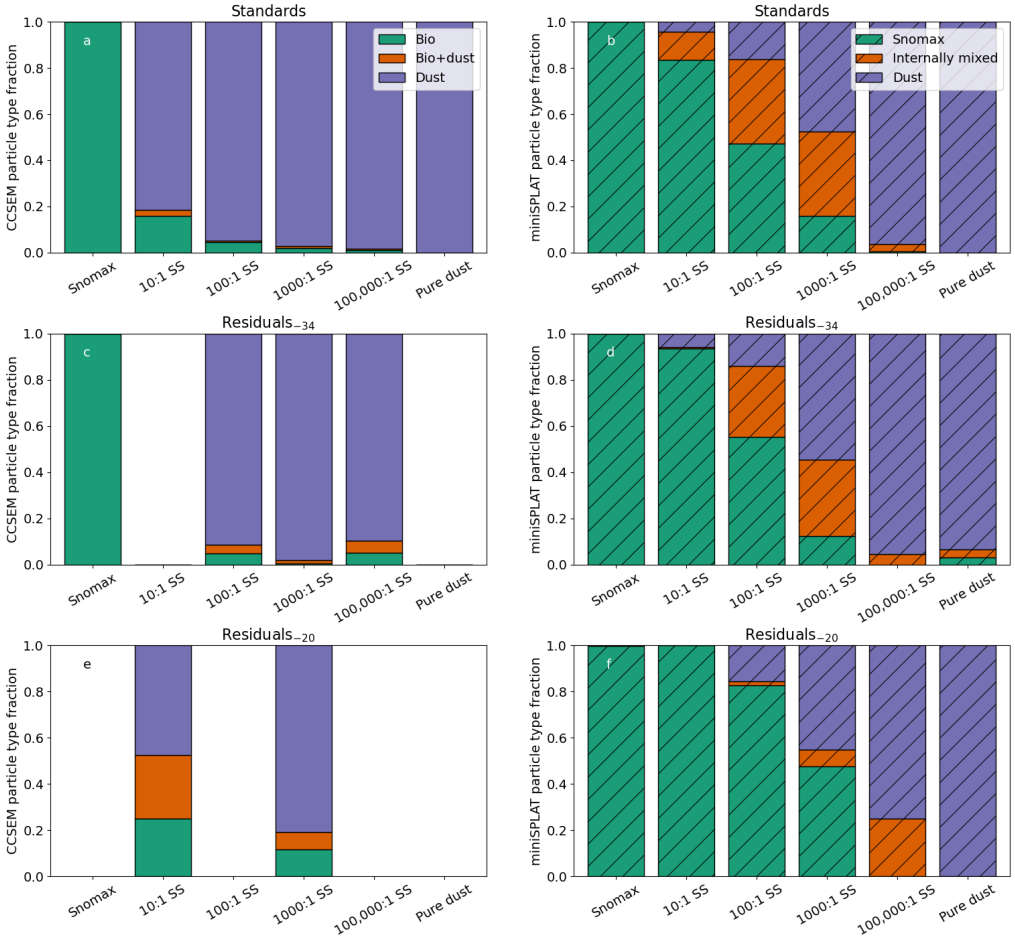

Figure 2. Fraction of particle classes as measured by CCSEM/EDX (left) and miniSPLAT (right) for standards (top row), residuals measured at -34 °C (middle row), and residuals measured at -20 °C (bottom row).

single particle mass spectra measured by the miniSPLAT showed clear differences between the synthetic soils. Figure 3 shows average positive mass spectra measured by the miniSPLAT for Snomax, synthetic soils, and dust particles. Snomax spectra are characterized by peaks previously tied to biological spectra including $^{18}NH_4^+$, $^{23}Na^+$, $^{30}NO^+$, $^{39}K^+$, $^{18}NH_4^+$ 43^+, 72^+, 84^+, and 86^+ (Cornwell et al., 2022), while dust particles are characterized by $^{39}K^+$, $^{44}SiO^+$, $^{73}Si_2OH^+$, $98^+/100^+$, and 147^+. Qualitatively, the synthetic soil spectra are quite sensitive to the presence of Snomax material. For instance, the

https://doi.org/10.5194/egusphere-2026-3882
Preprint. Discussion started: 27 July 2026

spectra of the 10:1, 100:1, and 1000:1 soils have mass spectral features that look similar to the pure Snomax, while it is only the 100,000:1 soil spectra that look similar to those of the pure dust (Fig. 3).

Our classification scheme identified miniSPLAT spectra as either (1) Snomax, (2) internally mixed, or (3) dust based upon the relative peak area (RPA) of the combined peaks of $84^+, 86^+$. We note that while previous studies have identified $^{26}CN^-$, $^{42}CNO^-$, and $^{79}PO_3^-$ as markers indicating that biological material is internally mixed with dust Creamean et al. (2013), we did not use these peaks because we did not observe negative spectra with all of our particles and thus would have artificially constrained our ability to detect biological material. We observed that the miniSPLAT classification resulted in many more particles being identified as pure Snomax (Fig. 2b). For example, nearly 90%, 60%, and 45% of the 10:1, 100:1, and 1000:1 soils, respectively, were classified as Snomax. One particle in the pure Snomax standard was actually classified as dust based upon the $84^+, 86^+$, though inspection of the spectra confirmed that the particle contained other biological peaks and none from dust. The majority of the remaining particles were internally mixed, with only a fraction classified as dust (1%, 3%, and 4%). It was only at the most extreme mixing ratio, 100,000:1, that we observed this relationship change, with only 1% of particles classified as Snomax and less than 10% as internally mixed. Altogether, these results suggest that the miniSPLAT is much more sensitive to the presence of biological material in individual particles than CCSEM/EDX.

The residual particles measured by the miniSPLAT also had enhanced markers for biological material. While it is difficult to distinguish this by looking at the average spectra in Figure 3, closer analysis of the summed RPA for $84^+, 86^+$ shows that they are enhanced in the residuals compared to standards (Fig. 4). For example, summed $84^+, 86^+$ for Snomax standard measurements was 0.150 ± 0.041, while for residuals at -34 °C it was 0.156 ± 0.046, and residuals at -20 °C it was 0.162 ± 0.064. This enhancement of Snomax in synthetic soil residuals is also reflected in the increased fraction of residual particles that are classified as either Snomax or internally mixed (Fig. 2). Our measurements of residual composition, from both the CCSEM/EDX and miniSPLAT, show that the components of the synthetic soils responsible for initiating ice nucleation are primarily derived from Snomax.

Another notable feature of the residual spectra is that the 98^+ and 100^+ peaks disappeared from the residual spectra of pure dust and the 100,000:1 soil (Fig. 3). To determine whether the disappearance of these peaks could be explained as the absence of ice nucleating materials, we conducted an additional set of experiments where we introduced montmorillonite to the PNNL-CFDC under conditions where particles activate into droplets, but not freeze into ice crystals (see Appendix A. For these experiments, we did not see these peaks at $98{,}100^+$ either, suggesting that their presence is either an artifact of the process used to create the synthetic soils or otherwise removed by the wetting process (Fig. A1).

We are ultimately interested in whether we have the measurement capabilities to predict INP concentrations from complex mixed particles from aerosol measurements. As such, it is imperative to understand the relative strengths and weaknesses of our characterization methods. One interesting result from these experiments is the disagreement between the mixing state between the CCSEM/EDX vs miniSPLAT. For instance, CCSEM/EDX classified synthetic soils as being primarily dust for all soils, while the miniSPLAT showed substantially more Snomax and internally mixed particle fractions (Fig. 2a-b). Previous studies have found that SEM may not capture internal mixing that other particles can. Using a volatility hygroscopicity tandem differential mobility analyzer (VH-TDMA), Augustin-Bauditz et al. (2016) were able to calculate that the average amount of

https://doi.org/10.5194/egusphere-2026-3882
Preprint. Discussion started: 27 July 2026

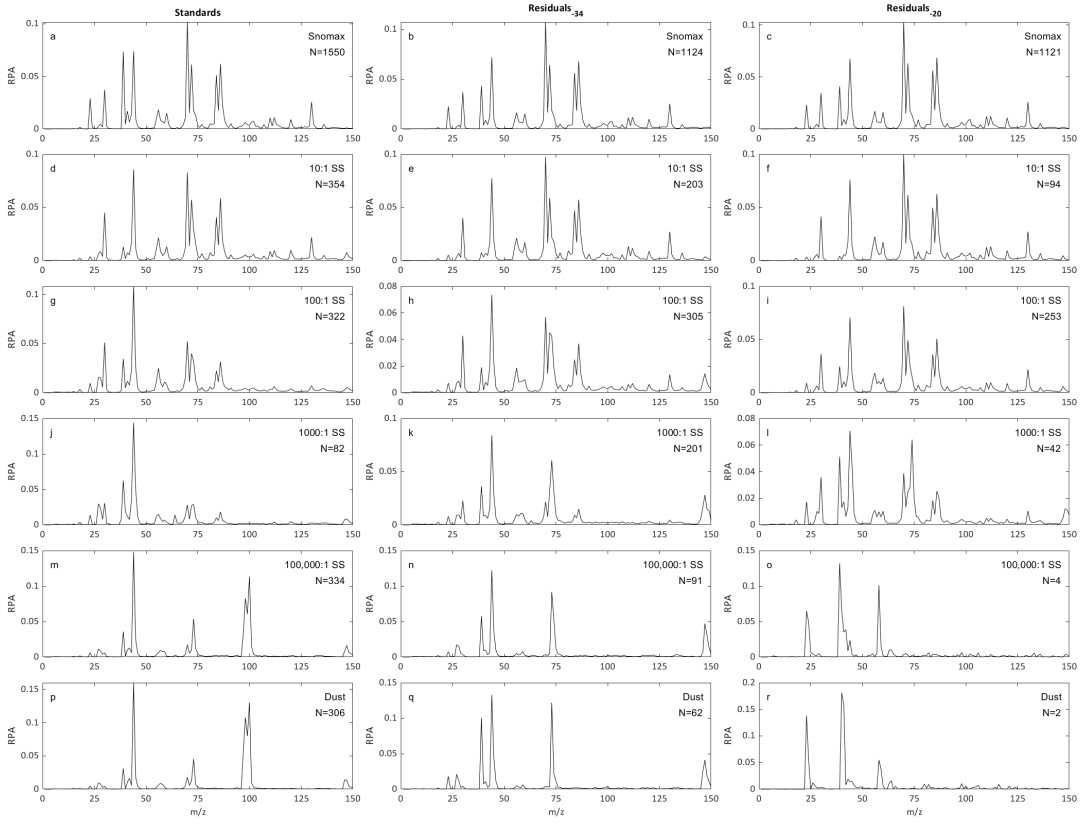

Figure 3. Average miniSPLAT spectra for size-selected synthetic soils. Each row corresponds to a different soil while the columns differ by the measurement type: standard measurements, residuals measured at -34 °C (Residuals$_{-34}$), and residuals measured at -20 °C (Residuals$_{-20}$).

birch pollen washing water on 500-nm size-selected illite particles was 9.7%. However, they were unable to detect evidence of internal mixing using CCSEM/EDX, which they attributed to the film of birch pollen washing water surrounding the illite (estimated at 8 nm) being too indistinct to be detected. We note that the detection limit of CCSEM/EDX is generally taken to be 0.1%, and the average P detected on pure Snomax particles was 0.68% (Table D1). Given that P is one of the primary ways we identify biological material, at even just 10% internal-mixing (and assuming that the P fraction scales linearly with concentration) most of these particles would be well under this threshold. Thus, we think it is plausible that CCSEM/EDX may fail to identify a significant fraction of internally mixed particles, resulting in under-predicted INP concentrations.

3.2 Particle size and shape

We measured the size, shape, and ρ_{eff} of synthetic soil standards using CCSEM/EDX and miniSPLAT. CCSEM/EDX estimates particle size by estimating the diameter and a shape score from the outline particles deposited on the substrate. The size distribution of the particles measured by the CCSEM/EDX was bimodal, with the primary mode peaking at ∼700 nm, and

https://doi.org/10.5194/egusphere-2026-3882
Preprint. Discussion started: 27 July 2026

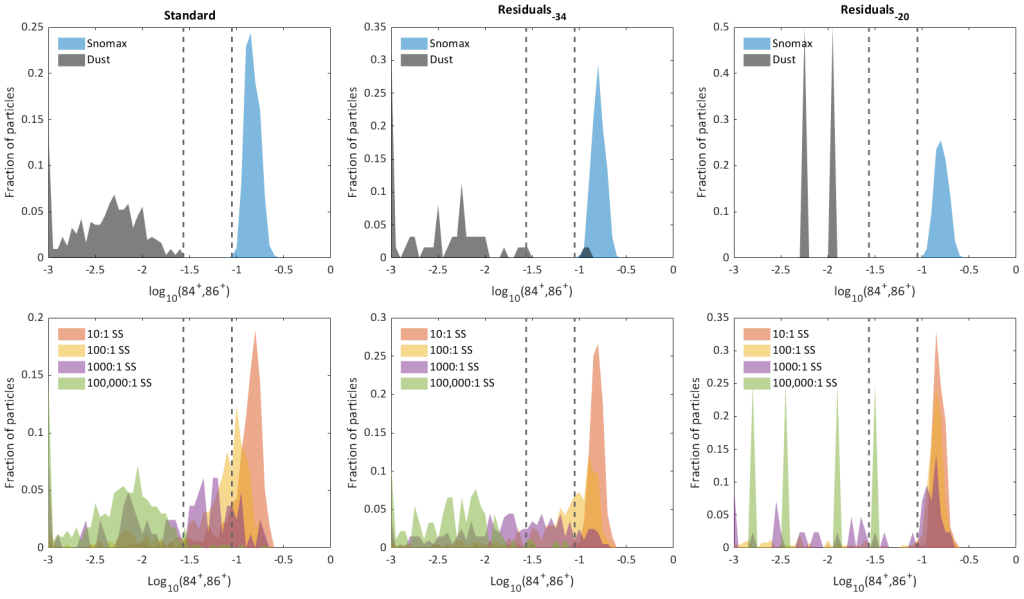

Figure 4. Histogram of summed $log_{10}(84^{+}, 86^{+})$ from miniSPLAT spectra for size-selected particles. The top row shows the distributions for pure Snomax and pure dust particles, while the bottom row shows the distributions for the synthetic soils. The columns differ by the measurement type: standard measurements, residuals measured at -34 °C (Residuals$_{-34}$), and residuals measured at -20 °C (Residuals$_{-20}$). The dashed lines show the cutoffs between "pure" and internally-mixed particles.

with all samples having a secondary mode at ∼200 nm (Fig. 5). Particle shapes for all standard measurements are mostly constrained to 2 and below, suggesting that most particles are nearly spherical, though in some instances they can approach values of 10. While all of the synthetic soil samples have relatively similar patterns of conjoined size and shape, only the 10:1 and 100,000:1 SS size distributions were statistically similar. See Appendix D for more detail on these statistical analyses. We were unable to collect sufficient samples for CCSEM/EDX analysis for some of our residual experiments, and thus our analysis remains incomplete. We note that for Snomax, residuals particles were not larger, while the average diameters for the synthetic soils were greater than for the standard particles (Table D1). This suggests that the factors controlling ice nucleation of pure Snomax are not governed by the particle size.

We used the vacuum aerodynamic diameter (d_{va}) of synthetic soil standards, measured by the miniSPLAT, to estimate the ρ_{eff} (see Appendix B for further details on these calculations). For all of the standard measurements, the particles exhibited smaller D_{va} compared to the D_a selected by the AAC, signifying smaller ρ_{eff} values (Fig. 6). We hypothesize that these low ρ_{eff} values are a result of the soil creation process either leading to irregularly shaped particles or introducing voids into the particles. We calculated Cohen's distance between the size distributions of each standard and observed that the synthetic soils were mostly shifted in sequence between dust and Snomax (Fig. D1), suggesting that adding Snomax modifies the concentration in a dose-dependent manner. Residual particles had enhanced D_{va} compared to the standards, leading to an increase in estimated

https://doi.org/10.5194/egusphere-2026-3882
Preprint. Discussion started: 27 July 2026

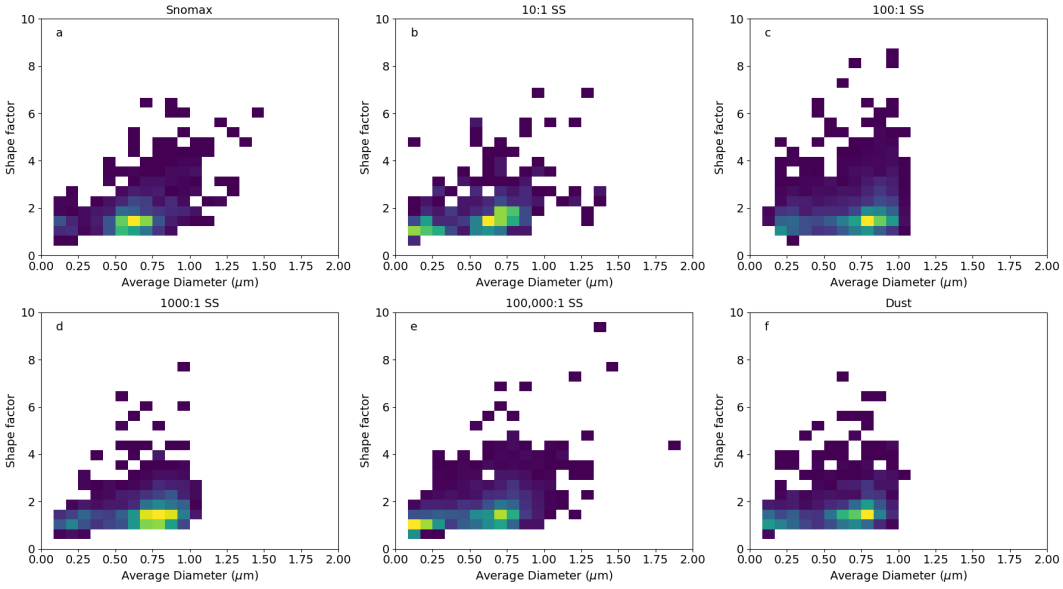

Figure 5. Joint distributions of the shape factor vs the average diameter measured by CCSEM/EDX for (a) pure Snomax; (b) 10:1 SS; 100:1 SS; 1000:1 SS, 100,000:1 SS, and pure dust.

ρ_{eff}, though this is not fully comparable given the inclusion of another potentially size-selective step (i.e. ice nucleation) in the chain of events.

Previous studies utilizing SPMS to study ice crystal residuals have found that the residuals were larger compared to the total particle population (Cornwell et al., 2019; Cziczo et al., 2006). These studies concluded that the increase in size for ice crystal residuals could be attributed to the well-established relationship between particle surface area (which is related to size) and ice nucleation activity (e.g. Niemand et al., 2012). We observe that the size distribution of Snomax particles could change simply by particle wetting and drying (Fig. A2). Given that we had a narrowly constrained size distribution, and that d_{va} is affected by density and shape in addition to physical diameter, these results imply that some of this shift in size distribution could be due to restructuring. We note that Mael et al., 2021 conducted water uptake experiments using micro-Raman spectroscopy and found no evidence of Snomax restructuring. However, in the CCSEM/EDX measurements presented here, Snomax particles did not exhibit increased size in residuals compared to standards (D1). Thus we think it is plausible, that in our case, some increase in d_{va} may be due to a change in shape, in addition to freezing.

3.3 Surface composition

We also used the ToF-SIMS to measure the surface chemistry of bulk (i.e. *not* size-selected) synthetic soil samples. We measured classified spectral features using principal component analysis (PCA), which is commonly used in ToF-SIMS analysis for data reduction, group separation, semi-quantitative analysis (Cheng et al., 2023; Li et al., 2023; Yao et al., 2017). The

https://doi.org/10.5194/egusphere-2026-3882
Preprint. Discussion started: 27 July 2026

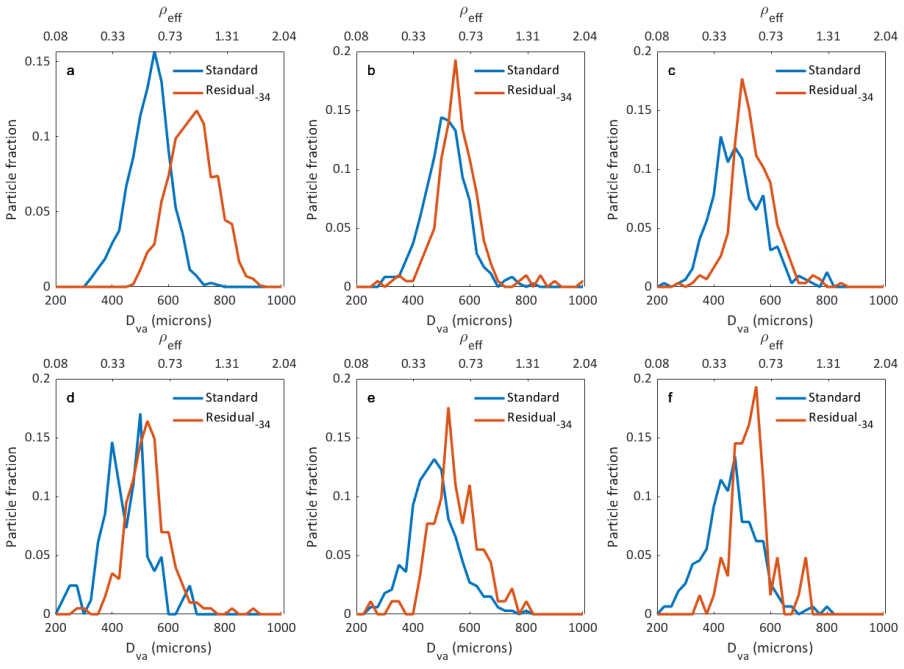

Figure 6. Probability distributions for particle D_{va} and ρ_{eff} as measured by the miniSPLAT. Plots are shown for (a) Snomax, (b) 10:1 SS, (c) 100:1 SS, (d) 1000:1 SS, (e) 100,000:1 SS, and (f) pure dust. Plots are shown for all particles (Standard; blue trace) and residuals measured at -34 °C ($Residual_{-34}$). The top axis shows the equivalent ρ_{eff} for a given diameter. We do not show the probability distributions for residuals measured at -20 °C due to their low sampling numbers.

negative ion PCA score plot (Fig. 7) shows good separation among the synthetic soils, with PC1 accounting for 97.2% of the total variance. The loading plot for PC1 (Fig. 8) shows the mass fragments contributing most significantly to PC1. Peaks with high loadings, such as m/z 79 (PO_3^-), 42 (CNO^-), and 97 (HSO_4^- or $H_2PO_4^-$) are more abundant in the soils with with higher Snomax content. These ions are associated with nitrogen-containing organics, SO_x, PO_x, and other organic acids, and are commonly found in studies of biological particles (Cornwell et al., 2022), and thus we interpret PC1 as corresponding to Snomax character. Peaks with high negative loadings, such as m/z 16 (O^-), 60/61 (SiO_2^-/SiO_2H^-) and 76 (SiO_3^-), are more prevalent in montmorillonite-rich samples, and reflect the silica-based composition of montmorillonite. We also performed a similar analysis using positive spectra, but it provided less distinct group separation compared to the negative spectral PCA. Therefore, for the rest of this manuscript we will refer to just the results from the negative spectral PCA.

To estimate the fractional surface coverage of Snomax on the synthetic soils ($A_{Sno,SS}$), we calculated the displacement of each soil along the PC1 axis relative to the pure Snomax and pure montmorillonite samples via the following

$$A_{Sno,SS} = \frac{R_{mont} - R_{SS}}{R_{mont} - R_{Snomax}},$$

https://doi.org/10.5194/egusphere-2026-3882
Preprint. Discussion started: 27 July 2026

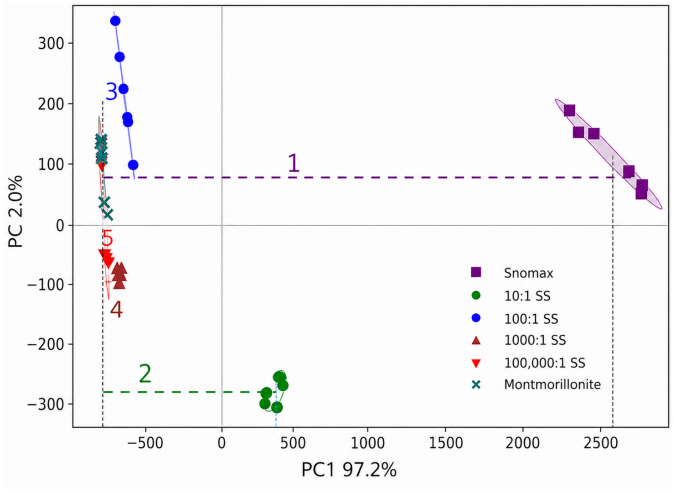

Figure 7. Score plot of negative spectral PCA from the ToF-SIMS analysis Shaded areas show the 95% confidence intervals and the dashed lines show the labeled distance along the PC1 coordinate.

where R_{SS} is the average value of the synthetic soil along PC1 score, R_{mont} is the average value of pure montmorillonite along PC1 score, and R_{Snomax} is the average value of pure Snomax along PC1 score. Table 4 shows the $A_{Sno,SS}$ for the synthetic soils. Together, the PCA scores and loadings demontrate clear compositional differences between sample groups, enabling differentiation and semi-quantitative analysis of $A_{Sno,SS}$. We note that these PCs are calculated for bulk particles and not the size-selected particles used in the rest of this analysis, and while they are not directly comparable to the other results, they still are our only estimate of the fractional surface coverage of Snomax. Similar to the other measurement techniques, the TOF-SIMS showed a non-linear relationship between the composition of the soils and their ostensible mixing ratio. For instance, the surface coverage from 10:1 to 100:1 declines by approximately an order of magnitude, and remains largely unchanged from 100:1 to 1000:1. This suggests that the soil generation process is not equally effective at coating particles across mixing ratios, which may explain why such a large fraction of particles remain externally mixed.

Sample	Negative spectra surface coverage (%)	Positive spectra surface coverage (%)
10:1 SS	33.7 (1.0)	42.8 (0.9)
100:1 SS	4.1 (0.5)	4.5 (0.3)
1000:1 SS	3.1 (0.2)	1.0 (0.4)
100,000:1 SS	0.2 (0.3)	N/A

Table 4. Surface coverage of Snomax on synthetic soil (SS) particles as determined by ToF-SIMS. Surface coverage calculated using both negative and positive spectra, and the uncertainty values are noted in parentheses. Values for pure dust and pure Snomax are not shown.

https://doi.org/10.5194/egusphere-2026-3882
Preprint. Discussion started: 27 July 2026

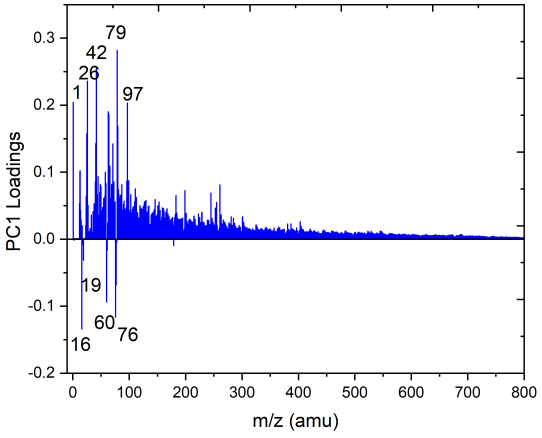

Figure 8. Loading plot for PC1, which shows the mass spectral peaks that directly contribute to PC1 (above zero) and those that inversely contribute (below zero).

3.4 Ice nucleation activity

We measured the IN activity of the synthetic soils using the PNNL-CFDC to test how mixing state affects synthetic soil ice nucleation propreties (Fig. 9a). At temperatures colder than 255 K, the samples containing Snomax had flat FF curves before rapidly increasing at temperatures < 243 K. We were unable to measure at temperatures warmer than 255 K due to the processing temperatures within the CFDC, and therefore we were unable to observe the relative freezing of the different ice nucleation protein complexes (e.g. Turner et al., 1990). Given that only Snomax-containing particles exhibit this "plateau", we assume that any ice nucleation occurring at these temperatures (or warmer) can be attributed to biological material. All particles containing montmorillonite exhibit a steep increase in frozen fraction at roughly 242-243 K, suggesting that this increase in IN-activity is likely to originate from montmorillonite. While we cannot conclusively rule out that Snomax may have contributed at these temperatures as well, we note that there is no corresponding change in the frozen fraction of the pure Snomax samples.

These results highlight the importance of the biological components of the synthetic soils in controlling their IN activity. To further investigate the relationship between mixing state and IN activity, we define a biological frozen fraction, f^*, that corresponds to the plateau observed in Figure 9a i.e. the IN activity coming from biological residues. We calculated f^* by averaging the frozen fraction between 250 and 253 K. Figure 9b shows f^* normalized to the f^* of pure Snomax ($\frac{f^*}{f^*_{sno}}$) plotted against the synthetic soil mixing ratio. If there was a linear relationship between the mass ratio of Snomax and the biological ice fraction, then the data would fall along the 1:1 line. However, $\frac{f^*}{f^*_{sno}}$ clearly does not scale with the mixing ratio, which we emphasize is not a measured property, but rather derived from the ratios of materials used to make the synthetic soils. We note that the relationship between $\frac{f^*}{f^*_{sno}}$ and $A_{\mathrm{Sno,SS}}$ follow similar trends in their relationship to the soil mixing ratio. We find

https://doi.org/10.5194/egusphere-2026-3882
Preprint. Discussion started: 27 July 2026

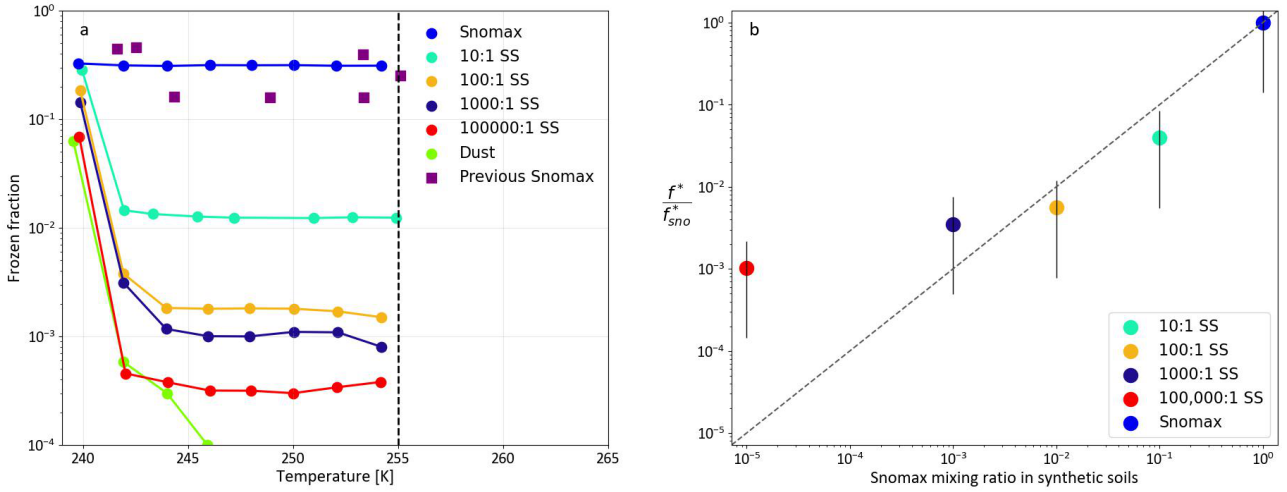

Figure 9. Ice nucleation measurements of synthetic soils: (a) frozen fraction vs the temperature for the synthetic soils, with frozen fraction values for Snomax from previous studies (Wex et al., 2015; Hartmann et al., 2013) shown in purple, and (b) biological frozen fraction normalized to Snomax ($\frac{f^*}{f^*_{sno}}$) vs Snomax mixing ratio. Grey dashed lines show the 1:1 line.

it quite plausible that Snomax is unevenly distributed across the size range of synthetic soil particles, which may explain the discrepancy between $\frac{f^*}{f^*_{sno}}$ and mixing ratio, though we have no direct evidence to support or refute this hypothesis.

3.5 Ice nucleation experiment simulations

We simulated INP concentrations as measured by the CFDC following the probabilistic approach utilized by Alpert and Knopf (2016). The primary difference between these simulations is the representation of the particle mixing state (i.e. the relative amounts of particles that are Snomax, dust, or internally mixed). We tested several approaches to determining mixing state: (1) mixing state is externally mixed, and determined by the mass mixing ratios used to make the synthetic soils; (2) mixing state is internally mixed, also determined by the mass mixing ratios; (3) a combination of internal and external mixtures where we assumed half of the Snomax mass was present in pure Snomax particles, and the other half was present in internally mixed particles; (4) particle mixing state is informed by CCSEM/EDX observations; (5) particle mixing state is informed by miniSPLAT observations; and (6) particle mixing state is informed by ToF-SIMS observations. Results are shown in Figure 10. The frozen fractions for all scenarios followed similar patterns to the CFDC simulations, with a plateau from 255 K before sharply increasing with decreasing temperature at around 243 K.

For the externally, internally, and combined external and internal mixture scenarios, the plateau fractions for these are very similar (Figure 10a-c). This may initially seem surprising, but is likely due to the fact that the ice nucleation activity at warm temperatures is ultimately controlled by the total mass of the Snomax in the particle population. Given that the mass is equal

https://doi.org/10.5194/egusphere-2026-3882
Preprint. Discussion started: 27 July 2026

in all three scenarios, and we assume that Snomax does not prevent dust from serving as an ice nuclei (i.e. by acting as in insoluble coating inhibiting the ice nucleation activity of dust), the freezing behavior should also be similar, with some minor deviations because of how the assumptions about mixing state impact the surface area of the dust core (see Appendix 2.5 for full details). Frozen fractions in the plateau region are over-estimated in the soils with more Snomax (10:1 and 100:1), and under-estimated in soils with less Snomax (1000:1 and 100,000:1). Additionally, frozen fractions at temperatures colder than 244 K are under-predicted across all samples. From these results we can conclude that bulk mixing ratio fails to predict the ice nucleation activity for the synthetic soils. We can also conclude that mixing state alone does not significantly affect the simulated ice fraction, as long as the total mass of Snomax is kept consistent between simulations.

We observed different values and patterns in simulated frozen fraction when we used observations to drive the simulated particle mixing state (Figure 10d-f). All simulations over-predicted f^*, while generally performing better at temperatures colder than 244 K. For both temperature regimes, the mismatch is likely due to the fact that they over-predict INP concentrations from Snomax rather than improved handling of freezing from dust. More specifically, the CCSEM/EDX does a better job of predicting plateau INP concentrations for soils with more Snomax (10:1, 100:1, and 1000:1), while the miniSPLAT does a better job when Snomax is low (100,000:1). These results are an extension of each analytical technique's sensitivity (or insensitivity in the case of CCSEM/EDX) to biological materials. The ToF-SIMS-informed simulation is able to better predict both the frozen fractions for soils containing low to moderate amounts of Snomax (100,000:1, 1000:1, and 100:1). However,the ToF-SIMS does not directly measure individual particles, but instead provides the average surface chemical composition across a large population of particles. Individual particles (and residual particles) may differ from this bulk mean property. This means that we are unable to directly link the results with the properties of the individual particles introduced to the CFDC, nor is there an ability to measure the composition of the residuals. Regardless, these results suggest that incorporating some information of particle mixing state from measurements may improve simulations of the freezing behavior under certain circumstances, though this varies both by the mixing state and analytical technique.

We considered several possible explanations for the lack of agreement between measured and simulated ice nucleation fractions. The first is that the adsorption of Snomax onto dust alters the ice nucleation activity of Snomax. Our only evidence of this is the discrepancy between the frozen fractions and the mixing ratios used to make the synthetic soils. We note that Augustin-Bauditz et al. (2016) and Beydoun et al. (2017) investigated the role of mixing state in the freezing of mixed dust-biological particles. Both studies determined that the freezing of mixed particles could be explained using multi-component models which assumed that the freezing of the dust and biological species was equal to that of the individual components. Given the lack of strong evidence for this explanation from our measurements, and that previous studies found it was not a factor, we conclude that the adsorption of Snomax onto dust altering its freezing activity is unlikely.

The second explanation is that the treatment of ice nucleation in our simulations is incorrect, and and which could include either faulty treatment of freezing and/or using non-representative parameterizations for the individual components. To rule out this possibility, we calculated the simulated particle type fraction using the experimental inputs for Residual-34 samples (Fig. 11). We wanted to test prediction in this temperature range because of the fact that both dust and Snomax are ice-active, because under our framework, dust is basically not ice-active at -20 °C. We assumed that if our treatment of ice nucleation was

https://doi.org/10.5194/egusphere-2026-3882
Preprint. Discussion started: 27 July 2026

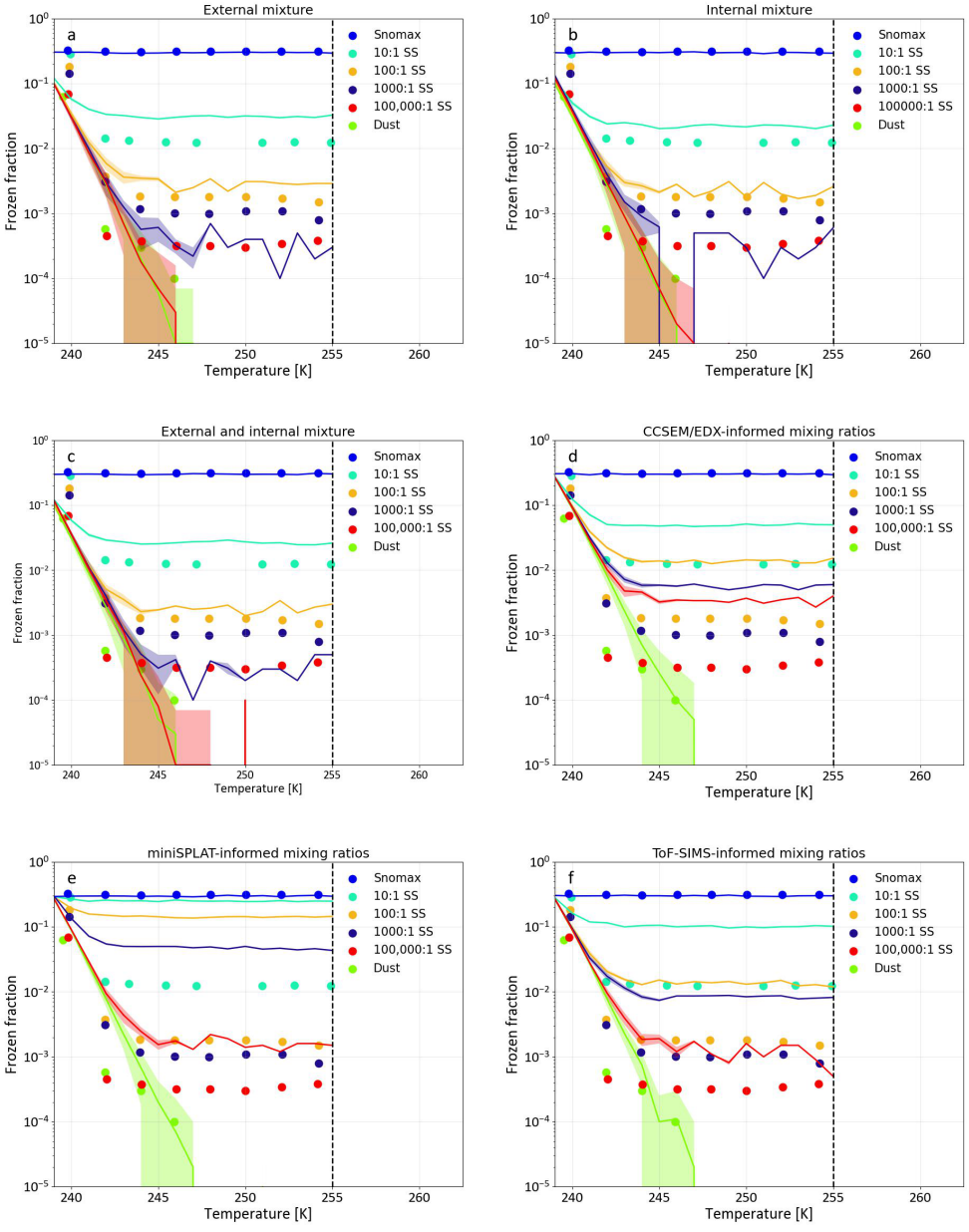

Figure 10. Simulated frozen fractions for CFDC experiments. Panels show the results for different assumptions about particle mixing state: (a) mass ratios are used to determine an externally mixed case; (b) mass ratios are used to determine an internally mixed case; (c) mass ratios are used to determine an externally and internally mixed case; (d) particle fractions determined by the CCSEM/EDX are used to determine the mixing state; (e) particle fractions determined by the miniSPLAT are used to determine the mixing state; and (f) particle fractions determined by the ToF-SIMS are used to determine the mixing state. Lines show simulated values with and shaded areas indicating the measurement uncertainty, while the circles show measurements from the PNNL-CFDC.

https://doi.org/10.5194/egusphere-2026-3882
Preprint. Discussion started: 27 July 2026

correct then the frozen fractions by type would be relatively similar to those from observations. With the CCSEM/EDX, we over-predicted the amount of Snomax and internally-mixed particles compared to the miniSPLAT observations, which were all primarily classified as dust. The miniSPLAT produced better agreement with internally-mixed particles, but generally over-predicted freezing from Snomax particles compared to dust. Given this qualitative agreement, we concluded that the treatment of freezing within our simulations was not the primary issue.

A third factor that could have been contributing to disagreement between simulated and measured frozen fractions would be the partitioning between the particle types. The frozen fraction of $\frac{f^*}{f^*_{sno}}$ is dictated by the relative fractions of Snomax and internally-mixed particles. Across the three experimentally-driven simulations particle concentrations, the relative fractions for Snomax-containing particles are consistently too high (Fig. 10). In the case of the miniSPLAT, this is not surprising given the apparent sensitivity of the instrument to Snomax on the soils. However, this is surprising for the CCSEM/EDX given that the relative lack of sensitivity. We suggest that perhaps both dust and Snomax are being incorrectly classified as pure components, when they are actually more internally-mixed. Given the asymmetry in the contribution of pure Snomax particles to frozen fractions, this would lead to decreased frozen fractions. From this, we can conclude that, *for this model system*, these analytical techniques are not well suited to resolving the differences in composition affecting ice nucleation activity. Additionally, the bulk mixing ratio fails to predict ice nucleation activity, and accurate prediction requires detailed mixing state on a per-particle basis.

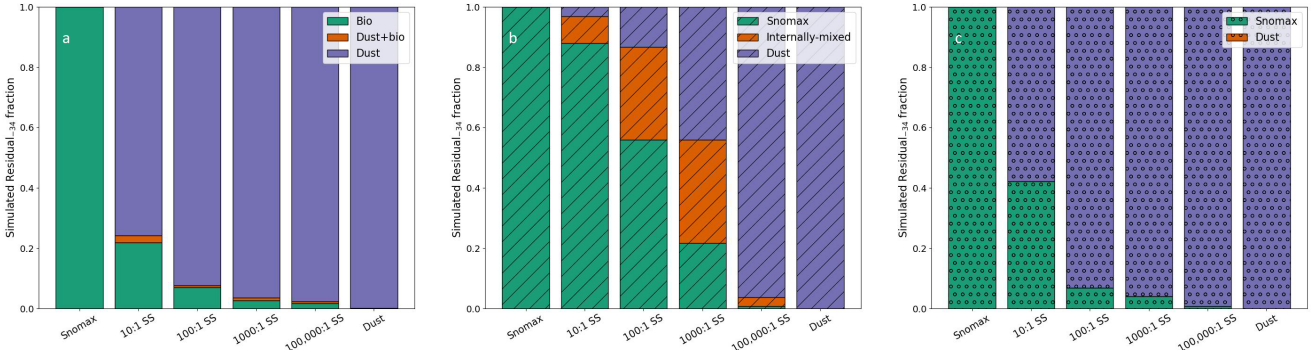

Figure 11. Simulated particle fractions of residuals$_{-34}$ for CFDC experiments using results from the (a) CCSEM/EDX, (b) miniSPLAT, and (c) ToF-SIMS.

4 Summary and conclusions

We generated synthetic soils using montmorillonite and Snomax and performed ice nucleation experiments wherein we characterized frozen fractions and INP composition to judge the suitability for current analytical methods for predicting complex particle mixtures. We used SPMS and CCSEM/EDX to characterize particle fractions of standard particles as well as residual particles measured at -34 and -20 °C, while the surface chemical composition of the soil particles was characterized using ToF-

https://doi.org/10.5194/egusphere-2026-3882
Preprint. Discussion started: 27 July 2026

SIMS. CCSEM/EDX primarily classifies particles as external mixtures of dust, which may be attributed to the fact that it lacks the sensitivity to detect internally-mixed dust particles beyond 10:1 mixing ratio. In contrast, the miniSPLAT is much more sensitive to Snomax and thus particles were classified as primarily Snomax or internally-mixed. Residual composition from both CCSEM/EDX and the miniSPLAT were found to have enhanced levels of biological markers and subsequently greater numbers of particles identified as either Bio or Dust + Bio. We measured the frozen fractions of the synthetic soils using a CFDC and observed that the frozen fractions did not follow the mass mixing ratios. Simulations of ice nucleation experiments show mixing state did not have a significant effect upon ice nucleation activity, as long as the total mass of Snomax was kept constant. We also found some limited evidence that incorporating particle mixing state from measurements improves simulations of the freezing behavior under certain circumstances, though the utility of each analytical technique varied by the mixing ratio.

In this study, we assessed our ability to establish aerosol-INP closure in a complex model system. This assessment was complicated by the fact that observed frozen fractions in the PNNL-CFDC did not follow the mass mixing ratio as expected. It is unclear if this is due to the fact that the Snomax on particles was unevenly distributed across the size range, the soil generation process did not work effectively across all samples, or if there is some more complicated interplay between dust and Snomax affecting the ice nucleation activity of these particles. We observed that our simulations were mostly insensitive to the assumptions about mixing state, and that the most important factor was the total amount of Snomax within the experiment. Thus accurate prediction appears to require better constraints on the actual Snomax burden in the size-selected aerosol and, for certain temperature ranges, its distribution across particles.

Whether an analytical technique can provide mixing state information that improves simulation will vary by model system. Using the observed particle fractions to inform simulations improved the predictive capabilities at colder temperatures, while the prediction at warmer temperatures were typically worse. However, miniSPLAT- and ToF-SIMS-informed simulations better predicted the frozen fraction for soils with the least amount of Snomax, which we attribute to the relative sensitivity of each instrument to Snomax. For systems where trace fragments of one substance on another particle type can drastically change the IN-activity (as in this study), we suggest that SPMS may provide more utility than CCSEM/EDX. In systems where the IN activity is less sensitive to the mixing state (e.g. some coatings), then CCSEM/EDX may be preferable. Future studies are needed to confirm whether these guidelines are warranted and to better constrain when bulk composition, surface composition, or particle-resolved mixing state each control the IN activity of complex mixtures. More broadly, these results suggest that measurement-model closure for mixed dust-biological INPs require constraints on the abundance and particle-level distribution of active biological material, rather than relying only on population-average or bulk mixing-ratio descriptions.

Data availability. All data needed to evaluate the conclusions in this study are present in the paper. All data used in this study will be made publicly available upon publication of this manuscript at data.pnnl.gov.

https://doi.org/10.5194/egusphere-2026-3882
Preprint. Discussion started: 27 July 2026

Appendix A: Water activation experiments

We performed an additional set of experiments to explore whether activation of particles into droplets in the CFDC affected particle composition or shape. The goal of these experiments was to disentangle whether changes in residual particle properties were a result of selectivity from ice nucleation, or changes from droplet activation and evaporation (e.g. particle restructuring). These experiments were conducted by generating particles, size-selecting them with the AAC, and then introducing them into the CFDC, where they were exposed to supersaturation and temperature conditions that would cause droplet activation, but not freezing (Fig. 1c).

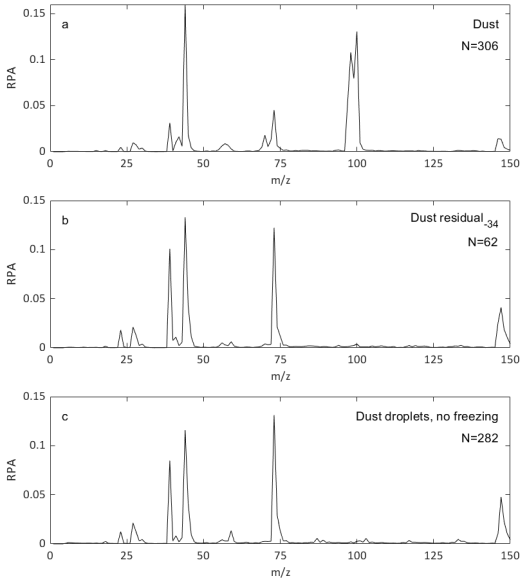

Figure A1. Average miniSPLAT spectra for dust particles from different experiments: panel a shows the average spectra from standards, panel b shows the average spectra from residuals measured at -34 °C, and panel c shows the average spectra from water activation experiments.

Figure A1 shows the average spectra from measurements of standard dust particles, residual particles, and dust particles from water activation experiments. The spectra from the residual and activation experiments are both missing the peaks at 98^+ and 100^+. Figure A2 shows the histograms of the d_{va} for standard particles, residual particles (measured at -34 °C), and particles from water activation experiments. Snomax standard particle size distribution shifts in size upon activation (yellow) and freezing (red), while dust does not.

Appendix B: Calculation of effective density from miniSPLAT measurements

The miniSPLAT was also used to calculated the effective densities (ρ_{eff}) for each sample. The aerodynamic diameter (d_a) of a particle is defined as the diameter of a sphere with standard density that settles at the same terminal velocity as the particle of

https://doi.org/10.5194/egusphere-2026-3882
Preprint. Discussion started: 27 July 2026

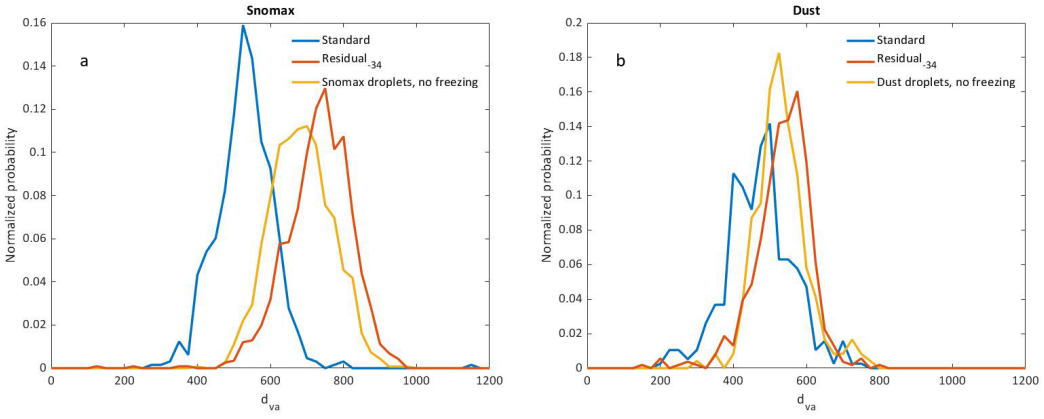

Figure A2. Average miniSPLAT spectra for dust particles from different experiments: panel a shows the average spectra from standards, panel b shows the average spectra from residuals measured at -34 °C, and panel c shows the average spectra from water activation experiments.

interest (DeCarlo et al., 2004). However, particle settling is affected by the drag force exerted by gas molecules surrounding the particles, and thus d_a is also dependent on the flow regime of the gas around the particle. The continuum regime (at or near atmospheric pressure) is where the surrounding gas can be thought of as a continuous fluid, whereas in the free-molecular regime (such as in a low pressure system in an instrument) the flow is likened to a series of collisions between the particle and gas molecules. Additionally, nonspherical particles experience increased drag compared to spherical particles and needs to be corrected for. This is accomplished using the dynamic shape factor, χ, which is defined as the ratio of drag on the nonspherical force to the drag on its volume equivalent sphere. The continuum regime aerodynamic diameter d_{ca} is described by the following

$$d_{ca} = d_{ve}\sqrt{\frac{\rho_p}{\rho_0 \chi_c}} \tag{B1}$$

Where d_{ve} is the volume equivalent diameter, ρ_p is the particle density, ρ_0 is standard density (1000 kg m^{-3}) and χ_c is the dynamic shape factor in the continuum regime. The vacuum aerodynamic diameter (d_{va}) is described by the following

$$d_{va} = \frac{d_{ve}}{\chi_v}\frac{\rho_p}{\rho_0} \tag{B2}$$

where χ_v is the dynamic shape factor in the free molecular regime. If we assume that $\chi_c \approx \chi_v$, then Eq. (B1) and Eq. (B2) can be rearranged to

$$\left(\frac{d_{va}}{d_{ca}}\right)^2 = \frac{\rho_p}{\chi \rho_0} \tag{B3}$$

The effective density of a particle, ρ_{eff}, can be described by

$$\rho_{\text{eff}} = \frac{\rho_p}{\chi} \tag{B4}$$

https://doi.org/10.5194/egusphere-2026-3882
Preprint. Discussion started: 27 July 2026

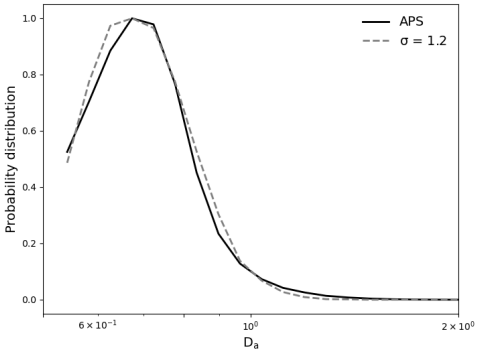

Figure B1. Aerodynamic diameter (D_a) distributions for particles selected by the AAC (measured by APS) and a log-normal distribution of simulated particles.

Eq. (B3) and Eq. (B4) can be rearranged to

$$\rho_{\text{eff}} = \left(\frac{d_{va}}{d_{ca}}\right)^2 \rho_0 \tag{B5}$$

In these experiments, we size-selected the d_{ca} of particles to be 700 nm using the AAC, while the d_{va} was measured using the miniSPLAT. Eq. (B1) can also be rearranged to

$$d_{ve} = d_{ca}\sqrt{\frac{\chi_c \rho_0}{\rho_p}} = d_{ca}\sqrt{\frac{\rho_0}{\rho_{\text{eff}}}} \tag{B6}$$

We use Eq. (B6) to calculate the d_{ve} for each synthetic soil to calculate the surface area and volume of each.

We assumed that the particle population exiting from the AAC was a log-normal distribution with a mean D_a of 700 nm and a geometric standard deviation of 1.2. Figure B1 shows that the simulated D_a distribution lines up well with the distribution measured by the APS.

Appendix C: Ice nucleation activities

We used a surface area-based parameterization for montmorillonite. Niemand et al. (2012) and subsequent studies have shown a strong relationship between particle surface area and the ice nucleation activity for different dust types. Ice nucleation activity has typically been parameterized from empirical fits of the active site density (n_s), a time-independent measure of ice nucleation activity. In our case, we use an empirical fit ($J_{\text{het}} = 10^{137.92-0.5331T}$), where T is the temperature in K, of the montmorillonite frozen fraction data for the J_{het} in our simulations.

Unlike dust, Snomax's ice nucleation activity does not appear to be related to its surface area. Hartmann et al. (2013) used a CFDC-type instrument to measure the ice nucleation activity of Snomax and observed that the frozen fraction plateaued at a temperature of roughly -15 °C. They attributed this plateau to the fact that not all Snomax particles contained the ice nucleation

https://doi.org/10.5194/egusphere-2026-3882
Preprint. Discussion started: 27 July 2026

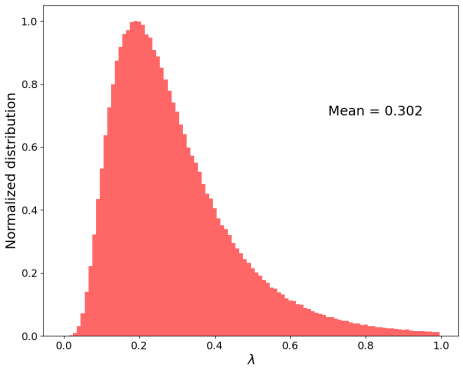

Figure C1. Probability distribution of corrected λ.

protein complexes responsible for its exceptionally warm freezing behavior. They derived a parameter, λ, that corresponded to to the likelihood a particle contains an INA protein complex, which was proportional to the particle volume. However, the ice nucleation activity of Snomax is not consistent between batches, and is also notoriously unstable (e.g. Polen et al., 2016), so we fit our λ to the frozen fraction of Snomax particles measured by the CFDC (Fig. C1), with the following

$$\lambda = 1.2069 \cdot 10^{-9} v \tag{C1}$$

where v is the particle volume with units of nm^3. We note in addition to calculating λ, Hartmann et al. (2013) also parameterized a temperature-dependent nucleation rate for particles that contained an ice nucleation protein complex. However, they observed a plateau at temperatures colder than $\sim$ -12 °C and inferred that at this temperature all possible biological INPs had frozen. Thus we assume that, at the temperatures that we are simulating, all particles with an ice nucleation protein complex freeze, and at the first step. Therefore, the probability of a particle containing Snomax will freeze is dependent upon λ.

We made several assumptions in or modeling of internally mixed particles. First, we assumed that particles were comprised of a core-shell morphology, with montmorillonite in the interior and Snomax on the outside. Second, we assumed that particles were internally mixed in a mass mixing ratio comparable to the mass mixing ratio used to make the synthetic soils. Finally, we assumed that the Snomax coating does not prevent the dust component in the soil from serving as the ice nucleating entity, and that both portions of the particle need to be modeled.

To calculate the ice nucleation activity of the two components, we require (1) the surface area inner dust core (a_i) and (2) the volume of the particle that is comprised of Snomax (v_o). To derive these properties, we first calculate a density of the total particle (ρ_t) using

$$\rho_t = \left(\frac{f_m}{\rho_i} + \frac{1 - f_m}{\rho_o} \right)^{-1} \tag{C2}$$

where f_m is the mass fraction of dust in the particle, ρ_i is the density of the inner core (dust), and ρ_o is the density of the outer coating (Snomax). Note that these are material specific densities, and not the same as the ρ_{eff} calculated from the miniSPLAT

https://doi.org/10.5194/egusphere-2026-3882
Preprint. Discussion started: 27 July 2026

measurements. From this information, we can calculate the total particle volume (v_t) using

$$v_t = \frac{\pi}{6} d_{ve}^3 \tag{C3}$$

Next, we calculate the total mass of the particle (m_t) with

$$m_t = v_t \rho_t \tag{C4}$$

This can be used to calculate the mass of the inner core (m_i) using

$$m_i = f_m m_t \tag{C5}$$

Then we calculate the volume of the inner core (v_i)

$$v_i = \frac{m_i}{\rho_i} \tag{C6}$$

where d_i is the inner (dust) core of the particle. We next calculate an inner radius (r_i) by

$$r_i = \sqrt[3]{\frac{3}{4\pi} v_i} \tag{C7}$$

Finally, we can calculate a_i by

$$a_i = 4\pi r_i^2 \tag{C8}$$

We calculate the outer volume (Snomax) of the particle by the following

$$v_o = v_t - v_i \tag{C9}$$

which we can use to calculate λ using equation C1 .

Appendix D: Statistical evaluation of particle distributions

To formally evaluate whether the size distributions for the different samples are similar, we apply the Kolmogorov-Smirnov (K-S) test to our samples. The K-S test is a robust statistical measure that can determine if a sample comes from a population with a specific distribution. This test is useful when the you cannot make assumptions about the shape of the underlying distributions.

Table D1 provides summary statistics for select properties measured by the CCSEM/EDX. We include the diameter, shape, and elemental fractions for markers used in identifying biological particles (P, C, N, O, S) and those prevalent in dust particles (Al, Si).

Acknowledgements. This research was supported by the Department of Energy (DOE), Office of Science, Office of Biological and Environmental Research through the Early Career Research program (KP1701010/72149; GC, IS, SB). GK, AZ, LF were supported by the

https://doi.org/10.5194/egusphere-2026-3882
Preprint. Discussion started: 27 July 2026

Sample	D_p (μm)	Shape	P (%)	C (%)	N (%)	O (%)	S (%)	Al (%)	Si (%)
Snomax Standard	0.63 ± 0.22	1.79 ± 0.94	0.68 ± 0.46	79.34 ± 3.49	7.30 ± 2.96	10.23 ± 2.90	0.51 ± 0.56	0.00 ± 0.01	0.07 ± 0.12
10:1 SS Standard	0.58 ± 0.27	1.89 ± 1.02	0.19 ± 0.32	45.96 ± 17.06	3.57 ± 4.29	33.55 ± 11.80	0.08 ± 0.15	2.18 ± 1.54	13.69 ± 7.29
100:1 SS Standard	0.66 ± 0.24	1.75 ± 0.79	0.01 ± 0.07	35.79 ± 12.26	0.51 ± 2.55	42.97 ± 8.99	0.00 ± 0.02	2.27 ± 1.70	18.35 ± 5.93
1000:1 SS Standard	0.67 ± 0.23	1.58 ± 0.67	0.01 ± 0.08	37.55 ± 13.72	0.23 ± 1.81	41.64 ± 9.77	0.00 ± 0.02	2.21 ± 1.86	18.29 ± 5.32
100,000:1 SS Standard	0.53 ± 0.28	1.62 ± 0.83	0.09 ± 0.14	43.38 ± 13.30	1.46 ± 0.91	35.38 ± 7.95	0.01 ± 0.04	2.63 ± 1.49	16.24 ± 4.87
Dust Standard	0.59 ± 0.25	1.66 ± 0.75	0.00 ± 0.03	39.32 ± 12.01	0.05 ± 0.37	39.69 ± 8.33	0.00 ± 0.00	2.37 ± 1.87	18.47 ± 4.24
Snomax residual (-34 °C)	0.64 ± 0.11	1.28 ± 0.50	0.90 ± 0.26	75.91 ± 4.17	7.20 ± 1.71	9.17 ± 1.75	0.94 ± 0.60	0.01 ± 0.03	0.25 ± 0.18
10:1 SS residual (-34 °C)	n/a	n/a	n/a	n/a	n/a	n/a	n/a	n/a	n/a
100:1 SS residual (-34 °C)	0.86 ± 0.34	1.76 ± 0.89	0.18 ± 0.16	48.31 ± 12.10	1.76 ± 1.10	31.46 ± 6.59	0.05 ± 0.09	2.43 ± 1.04	14.62 ± 4.67
1000:1 SS residual (-34 °C)	0.83 ± 0.35	2.02 ± 1.09	0.19 ± 0.15	40.02 ± 11.74	1.71 ± 0.73	36.67 ± 6.93	0.02 ± 0.05	2.93 ± 1.30	17.35 ± 4.11
100,000:1 SS residual (-34 °C)	0.88 ± 0.43	2.07 ± 1.62	0.18 ± 0.15	44.88 ± 15.12	1.55 ± 0.71	33.97 ± 8.20	0.05 ± 0.08	2.68 ± 1.09	15.55 ± 5.32
Dust residual (-34 °C)	n/a	n/a	n/a	n/a	n/a	n/a	n/a	n/a	n/a
Snomax residual (-20 °C)	n/a	n/a	n/a	n/a	n/a	n/a	n/a	n/a	n/a
10:1 SS residual (-20 °C)	0.83 ± 0.29	1.42 ± 0.81	0.51 ± 0.36	61.93 ± 15.21	5.53 ± 2.75	21.68 ± 9.99	0.14 ± 0.14	1.40 ± 1.31	8.27 ± 6.12
100:1 SS residual (-20 °C)	n/a	n/a	n/a	n/a	n/a	n/a	n/a	n/a	n/a
1000:1 SS residual (-20 °C)	0.81 ± 0.40	1.42 ± 1.03	0.17 ± 0.23	52.05 ± 16.59	2.85 ± 1.73	28.18 ± 10.46	0.19 ± 0.38	3.28 ± 4.10	11.20 ± 5.96
100,000:1 SS residual (-20 °C)	n/a	n/a	n/a	n/a	n/a	n/a	n/a	n/a	n/a
Dust residual (-20 °C)	n/a	n/a	n/a	n/a	n/a	n/a	n/a	n/a	n/a

Table D1. Particle means and standard deviations for select properties measured by CCSEM/EDX.

https://doi.org/10.5194/egusphere-2026-3882
Preprint. Discussion started: 27 July 2026

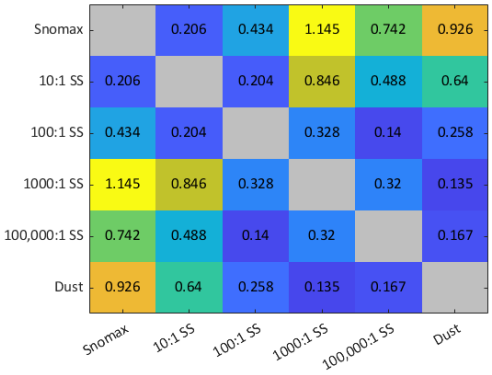

Figure D1. Cohen's distance for size distributions measured by the miniSPLAT between standard and residuals.

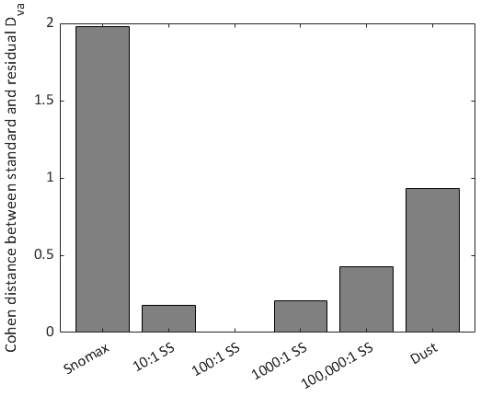

Figure D2. Cohen's distance between size distributions measured by the miniSPLAT for the synthetic soil standards. Color shows intensity and the value is given for each cell. Grey shaded area denotes comparisons between the same sample.

Atmospheric System Research (ASR) program as part of the DOE Office of Biological and Environmental Research under PNNL project KP1701010/57131. The Pacific Northwest National Laboratory is operated for DOE by Battelle Memorial Institute under contract DE-1713 AC05-76RL01830. A portion of this research was performed on project award (10.46936/lser.proj.2022.60392/60008564) and used resources at the Environmental Molecular Sciences Laboratory (EMSL), which is a DOE Office of Science User Facility and sponsored by the Biological and Environmental Research program.

https://doi.org/10.5194/egusphere-2026-3882
Preprint. Discussion started: 27 July 2026

References

Alpert, P. A. and Knopf, D. A.: Analysis of isothermal and cooling-rate-dependent immersion freezing by a unifying stochastic ice nucleation model, Atmospheric Chemistry and Physics, 16, 2083–2107, https://doi.org/10.5194/acp-16-2083-2016, publisher: Copernicus GmbH, 2016.

Augustin-Bauditz, S., Wex, H., Kanter, S., Ebert, M., Niedermeier, D., Stolz, F., Prager, A., and Stratmann, F.: The immersion mode ice nucleation behavior of mineral dusts: A comparison of different pure and surface modified dusts, Geophysical Research Letters, 41, 7375–7382, https://doi.org/10.1002/2014GL061317, 2014.

Augustin-Bauditz, S., Wex, H., Denjean, C., Hartmann, S., Schneider, J., Schmidt, S., Ebert, M., and Stratmann, F.: Laboratory-generated mixtures of mineral dust particles with biological substances: Characterization of the particle mixing state and immersion freezing behavior, Atmospheric Chemistry and Physics, 16, 5531–5543, https://doi.org/10.5194/acp-16-5531-2016, 2016.

Beydoun, H., Polen, M., and Sullivan, R. C.: A new multicomponent heterogeneous ice nucleation model and its application to Snomax bacterial particles and a Snomax–illite mineral particle mixture, Atmospheric Chemistry and Physics, 17, 13 545–13 557, https://doi.org/10.5194/acp-17-13545-2017, publisher: Copernicus GmbH, 2017.

Boulter, J. E., Cziczo, D. J., Middlebrook, a. M., Thomson, D. S., and Murphy, D. M.: Design and Performance of a Pumped Counterflow Virtual Impactor, Aerosol Science and Technology, 40, 969–976, https://doi.org/10.1080/02786820600840984, iSBN: 0278-6826, 2006.

Burrows, S. M., McCluskey, C. S., Cornwell, G., Steinke, I., Zhang, K., Zhao, B., Zawadowicz, M., Raman, A., Kulkarni, G., China, S., Zelenyuk, A., and DeMott, P. J.: Ice-Nucleating Particles That Impact Clouds and Climate: Observational and Modeling Research Needs, Reviews of Geophysics, 60, e2021RG000 745, https://doi.org/10.1029/2021RG000745, 2022.

Cheng, C., Zhou, Y., Nelson, H. M., Ahmadullah, T., Piao, H., Wang, Z., Guo, W., Wang, J.-G., Lai, G., and Zhu, Z.: Molecular identification of wines using in situ liquid SIMS and PCA analysis, Frontiers in Chemistry, 11, https://doi.org/10.3389/fchem.2023.1124229, publisher: Frontiers, 2023.

Cheng, Z., Morgenstern, M., Zhang, B., Fraund, M., Lata, N. N., Brimberry, R., Marcus, M. A., Mazzoleni, L., Fialho, P., Henning, S., Wehner, B., Mazzoleni, C., and China, S.: Particle phase-state variability in the North Atlantic free troposphere during summertime is determined by atmospheric transport patterns and sources, Atmospheric Chemistry and Physics, 22, 9033–9057, https://doi.org/10.5194/acp-22-9033-2022, 2022.

Conen, F., Morris, C. E., Leifeld, J., Yakutin, M. V., and Alewell, C.: Biological residues define the ice nucleation properties of soil dust, Atmospheric Chemistry and Physics, 11, 9643–9648, https://doi.org/10.5194/acp-11-9643-2011, iSBN: 1680-7324, 2011.

Cornwell, G. C., McCluskey, C. S., Levin, E. J. T., Suski, K. J., DeMott, P. J., Kreidenweis, S. M., and Prather, K. A.: Direct Online Mass Spectrometry Measurements of Ice Nucleating Particles at a California Coastal Site, Journal of Geophysical Research: Atmospheres, 124, 12 157–12 172, https://doi.org/10.1029/2019JD030466, 2019.

Cornwell, G. C., Sultana, C. M., Petters, M. D., Al-Mashat, H., Rothfuss, N. E., Möhler, O., DeMott, P. J., Martin, A. C., and Prather, K. A.: Discrimination between individual dust and bioparticles using aerosol time-of-flight mass spectrometry, Aerosol Science and Technology, 56, 592–608, https://doi.org/10.1080/02786826.2022.2055994, 2022.

Cornwell, G. C., McCluskey, C. S., Hill, T. C., Levin, E. T., Rothfuss, N. E., Tai, S.-L., Petters, M. D., DeMott, P. J., Kreidenweis, S., Prather, K. A., and Burrows, S. M.: Bioaerosols are the dominant source of warm-temperature immersion-mode INPs and drive uncertainties in INP predictability, Science Advances, 9, eadg3715, https://doi.org/10.1126/sciadv.adg3715, publisher: American Association for the Advancement of Science, 2023.

https://doi.org/10.5194/egusphere-2026-3882
Preprint. Discussion started: 27 July 2026

Cornwell, G. C., Steinke, I., Lata, N. N., Zelenyuk, A., Kulkarni, G., Pekour, M., Perkins, R., Levin, E. J. T., China, S., DeMott, P. J., and Burrows, S. M.: Enrichment of Phosphates, Lead, and Mixed Soil-Organic Particles in INPs at the Southern Great Plains Site, Journal of Geophysical Research: Atmospheres, 129, e2024JD040 826, https://doi.org/10.1029/2024JD040826, 2024.

Creamean, J. M., Suski, K. J., Rosenfeld, D., Cazorla, A., DeMott, P. J., Sullivan, R. C., White, A. B., Ralph, F. M., Minnis, P., Comstock, J. M., Tomlinson, J. M., and Prather, K. a.: Dust and biological aerosols from the Sahara and Asia influence precipitation in the western U.S., Science, 339, 1572–8, https://doi.org/10.1126/science.1227279, ISBN: 0036-8075, 2013.

Cziczo, D. J., Thomson, D. S., Thompson, T. L., DeMott, P. J., and Murphy, D. M.: Particle analysis by laser mass spectrometry (PALMS) studies of ice nuclei and other low number density particles, International Journal of Mass Spectrometry, 258, 21–29, https://doi.org/10.1016/j.ijms.2006.05.013, 2006.

DeCarlo, P. F., Slowik, J. G., Worsnop, D. R., Davidovits, P., and Jimenez, J. L.: Particle Morphology and Density Characterization by Combined Mobility and Aerodynamic Diameter Measurements. Part 1: Theory, Aerosol Science and Technology, 38, 1185–1205, https://doi.org/10.1080/027868290903907, 2004.

Gunsch, M. J., Kirpes, R. M., Kolesar, K. R., Barrett, T. E., China, S., Sheesley, R. J., Laskin, A., Wiedensohler, A., Tuch, T., and Pratt, K. A.: Contributions of transported Prudhoe Bay oil field emissions to the aerosol population in Utqiaġvik, Alaska, Atmospheric Chemistry and Physics, 17, 10 879–10 892, https://doi.org/10.5194/acp-17-10879-2017, 2017.

Gute, E., David, R. O., Kanji, Z. A., and Abbatt, J. P. D.: Ice Nucleation Ability of Tree Pollen Altered by Atmospheric Processing, ACS Earth and Space Chemistry, 4, 2312–2319, https://doi.org/10.1021/acsearthspacechem.0c00218, 2020.

Hartmann, S., Augustin, S., Clauss, T., Wex, H., Šantl Temkiv, T., Voigtländer, J., Niedermeier, D., and Stratmann, F.: Immersion freezing of ice nucleation active protein complexes, Atmospheric Chemistry and Physics, 13, 5751–5766, https://doi.org/10.5194/acp-13-5751-2013, publisher: Copernicus GmbH, 2013.

Hill, T. C. J., DeMott, P. J., Tobo, Y., Fröhlich-Nowoisky, J., Moffett, B. F., Franc, G. D., and Kreidenweis, S. M.: Sources of organic ice nucleating particles in soils, Atmospheric Chemistry and Physics, 16, 7195–7211, https://doi.org/10.5194/acp-16-7195-2016, 2016.

Huang, L., Yu, Q., Liu, W., Wang, J., Guo, W., Jia, E., Zeng, Q., Qin, R., Zheng, J., Hofmockel, K. S., Dong, H., Jiang, H., and Zhu, Z.: Molecular Determination of Organic Adsorption Sites on Smectite during Fe Redox Processes Using ToF-SIMS Analysis, Environmental Science & Technology, 55, 7123–7134, https://doi.org/10.1021/acs.est.0c08407, 2021.

Jahl, L. G., Brubaker, T. A., Polen, M. J., Jahn, L. G., Cain, K. P., Bowers, B. B., Fahy, W. D., Graves, S., and Sullivan, R. C.: Atmospheric aging enhances the ice nucleation ability of biomass-burning aerosol, Science Advances, 7, eabd3440, https://doi.org/10.1126/sciadv.abd3440, 2021.

Kanji, Z. A., Ladino, L. A., Wex, H., Boose, Y., Burkert-Kohn, M., Cziczo, D. J., and Krämer, M.: Overview of Ice Nucleating Particles, Meteorological Monographs, 58, 1.1–1.33, https://doi.org/10.1175/AMSMONOGRAPHS-D-16-0006.1, 2017.

Knopf, D. A., Alpert, P. A., Zipori, A., Reicher, N., and Rudich, Y.: Stochastic nucleation processes and substrate abundance explain time-dependent freezing in supercooled droplets, npj Climate and Atmospheric Science, 3, 1–9, publisher: Nature Publishing Group, 2020.

Kulkarni, G., Pekour, M., Afchine, A., Murphy, D. M., and Cziczo, D. J.: Comparison of Experimental and Numerical Studies of the Performance Characteristics of a Pumped Counterflow Virtual Impactor, Aerosol Science and Technology, 45, 382–392, https://doi.org/10.1080/02786826.2010.539291, 2011.

Kulkarni, G., Sanders, C., Zhang, K., Liu, X., and Zhao, C.: Ice nucleation of bare and sulfuric acid-coated mineral dust particles and implication for cloud properties: Ice formation on dust particles, Journal of Geophysical Research: Atmospheres, 119, 9993–10 011, https://doi.org/10.1002/2014JD021567, 2014.

https://doi.org/10.5194/egusphere-2026-3882
Preprint. Discussion started: 27 July 2026

Kulkarni, G., Zhang, K., Zhao, C., Nandasiri, M., Shutthanandan, V., Liu, X., Fast, J., and Berg, L.: Ice formation on nitric acid-coated dust particles: Laboratory and modeling studies, Journal of Geophysical Research: Atmospheres, 120, 7682–7698, https://doi.org/10.1002/2014JD022637, 2015.

Kulkarni, G., Hiranuma, N., Möhler, O., Höhler, K., China, S., Cziczo, D. J., and DeMott, P. J.: A new method for operating a continuous-flow diffusion chamber to investigate immersion freezing: assessment and performance study, Atmospheric Measurement Techniques, 13, 6631–6643, https://doi.org/10.5194/amt-13-6631-2020, 2020.

Laskin, A.: Electron Beam Analysis and Microscopy of Individual Particles, in: Fundamentals and Applications in Aerosol Spectroscopy, edited by Signorell, R. and Reid, J., pp. 463–491, CRC Press, https://doi.org/10.1201/b10417-23, 2011.

Laskin, A., Cowin, J., and Iedema, M.: Analysis of individual environmental particles using modern methods of electron microscopy and X-ray microanalysis, Journal of Electron Spectroscopy and Related Phenomena, 150, 260–274, https://doi.org/10.1016/j.elspec.2005.06.008, 2006.

Lata, N. N., Zhang, B., Schum, S., Mazzoleni, L., Brimberry, R., Marcus, M. A., Cantrell, W. H., Fialho, P., Mazzoleni, C., and China, S.: Aerosol Composition, Mixing State, and Phase State of Free Tropospheric Particles and Their Role in Ice Cloud Formation, ACS Earth and Space Chemistry, 5, 3499–3510, https://doi.org/10.1021/acsearthspacechem.1c00315, 2021.

Li, Y., Zhou, Y., Guo, W., Zhang, X., Huang, Y., He, E., Li, R., Yan, B., Wang, H., Mei, F., Liu, M., and Zhu, Z.: Molecular Imaging Reveals Two Distinct Mixing States of PM2.5 Particles Sampled in a Typical Beijing Winter Pollution Case, Environmental Science & Technology, 57, 6273–6283, https://doi.org/10.1021/acs.est.2c08694, publisher: American Chemical Society, 2023.

Mael, L. E., Busse, H. L., Peiker, G., and Grassian, V. H.: Low-Temperature Water Uptake of Individual Marine and Biologically Relevant Atmospheric Particles Using Micro-Raman Spectroscopy, The Journal of Physical Chemistry A, 125, 9691–9699, https://doi.org/10.1021/acs.jpca.1c08037, 2021.

Martin, A. C., Cornwell, G. C., Atwood, S. A., Moore, K. A., Rothfuss, N. E., Taylor, H., DeMott, P. J., Kreidenweis, S. M., Petters, M. D., and Prather, K. A.: Transport of pollution to a remote coastal site during gap flow from California's interior: impacts on aerosol composition, clouds, and radiative balance, Atmospheric Chemistry and Physics, 17, 1491–1509, https://doi.org/10.5194/acp-17-1491-2017, 2017.

Niemand, M., Möhler, O., Vogel, B., Vogel, H., Hoose, C., Connolly, P., Klein, H., Bingemer, H., DeMott, P., Skrotzki, J., and Leisner, T.: A Particle-Surface-Area-Based Parameterization of Immersion Freezing on Desert Dust Particles, Journal of the Atmospheric Sciences, 69, 3077–3092, https://doi.org/10.1175/JAS-D-11-0249.1, iSBN: 0022-4928, 2012.

Polen, M., Lawlis, E., and Sullivan, R. C.: The unstable ice nucleation properties of Snomax® bacterial particles, Journal of Geophysical Research: Atmospheres, 121, 11,666–11,678, https://doi.org/10.1002/2016JD025251, 2016.

Riemer, N., Ault, A. P., West, M., Craig, R. L., and Curtis, J. H.: Aerosol Mixing State: Measurements, Modeling, and Impacts, Reviews of Geophysics, 57, 187–249, https://doi.org/10.1029/2018RG000615, 2019.

Sultana, C. M., Cornwell, G. C., Rodriguez, P., and Prather, K. A.: FATES: a flexible analysis toolkit for the exploration of single-particle mass spectrometer data, Atmospheric Measurement Techniques, 10, 1323–1334, https://doi.org/10.5194/amt-10-1323-2017, 2017.

Tobo, Y., DeMott, P. J., Hill, T. C. J., Prenni, A. J., Swoboda-Colberg, N. G., Franc, G. D., and Kreidenweis, S. M.: Organic matter matters for ice nuclei of agricultural soil origin, Atmospheric Chemistry and Physics, 14, 8521–8531, https://doi.org/10.5194/acp-14-8521-2014, 2014.

Turner, M. A., Arellano, F., and Kozloff, L. M.: Three separate classes of bacterial ice nucleation structures., Journal of Bacteriology, 172, 2521–2526, https://doi.org/10.1128/jb.172.5.2521-2526.1990, 1990.

https://doi.org/10.5194/egusphere-2026-3882
Preprint. Discussion started: 27 July 2026

USDOE Office of Science (SC), Biological and Environmental Research (BER), Pacific Northwest National Laboratory (PNNL), Richland, WA (United States), Burrows, S., Barahona, D., Bertram, A., Chen, S., Diao, M., Fan, J., Fierce, L., French, J., Fridlind, A., Kanji, Z., Kollias, P., Korolev, A., Laskin, A., Liu, X., McCluskey, C., Möhler, O., Ovchinnikov, M., Phillips, V., Shaw, R., Shupe, M., Silber, I., Stratmann, F., Tan, I., Yang, F., Zhang, K., and Zheng, X.: Atmospheric System Research Workshop Report: New Directions in Atmospheric Ice Processes Research, Tech. Rep. DOE/SC-2023, 3030696, DOE, https://doi.org/10.2172/3030696, 2026.

Wex, H., Augustin-Bauditz, S., Boose, Y., Budke, C., Curtius, J., Diehl, K., Dreyer, A., Frank, F., Hartmann, S., Hiranuma, N., Jantsch, E., Kanji, Z. A., Kiselev, A., Koop, T., Möhler, O., Niedermeier, D., Nillius, B., Rösch, M., Rose, D., Schmidt, C., Steinke, I., and Stratmann, F.: Intercomparing different devices for the investigation of ice nucleating particles using Snomax® as test substance, Atmospheric Chemistry and Physics, 15, 1463–1485, https://doi.org/10.5194/acp-15-1463-2015, 2015.

Yao, J., Lao, D. B., Sui, X., Zhou, Y., Nune, S. K., Ma, X., Troy, T. P., Ahmed, M., Zhu, Z., Heldebrant, D. J., and Yu, X.-Y.: Two coexisting liquid phases in switchable ionic liquids, Physical Chemistry Chemical Physics, 19, 22 627–22 632, https://doi.org/10.1039/C7CP03754F, 2017.

Zelenyuk, A., Yang, J., Choi, E., and Imre, D.: SPLAT II: An Aircraft Compatible, Ultra-Sensitive, High Precision Instrument for In-Situ Characterization of the Size and Composition of Fine and Ultrafine Particles, Aerosol Science and Technology, 43, 411–424, https://doi.org/10.1080/02786820802709243, 2009.

Zhou, Y., Jiang, P., Chen, P., Jia, E., Welch, C. S., Zhao, Q., Dhas, J. A., Graham, E. B., Chen, X., Zhang, X., and Zhu, Z.: Novel principal component analysis tool based on python for analysis of complex spectra of time-of-flight secondary ion mass spectrometry, Journal of Vacuum Science & Technology A, 42, 023 204, https://doi.org/10.1116/6.0003355, 2024.

Zhu, C., Wang, Q., Huang, X., Yun, J., Hu, Q., and Yang, G.: Adsorption of amino acids at clay surfaces and implication for biochemical reactions: Role and impact of surface charges, Colloids and Surfaces B: Biointerfaces, 183, 110 458, https://doi.org/10.1016/j.colsurfb.2019.110458, 2019.